The Plant Cell, Vol. 19: 3669–3691, November 2007, www.plantcell.org © 2007 American Society of Plant Biologists

Downregulation of Cinnamoyl-Coenzyme A Reductase in Poplar: Multiple-Level Phenotyping Reveals Effects on Cell Wall Polymer Metabolism and Structure [W]

Jean-Charles Leplé,[a,b,c,1] Rebecca Dauwe,[a,b,1] Kris Morreel,[a,b,1] Véronique Storme,[a,b] Catherine Lapierre,[d] Brigitte Pollet,[d] Annette Naumann,[e] Kyu-Young Kang,[f,2] Hoon Kim,[g] Katia Ruel,[h] Andrée Lefèbvre,[h] Jean-Paul Joseleau,[h] Jacqueline Grima-Pettenati,[i] Riet De Rycke,[a,b] Sara Andersson-Gunneråas,[j] Alexander Erban,[k] Ines Fehrle,[k] Michel Petit-Conil,[l] Joachim Kopka,[k] Andrea Polle,[e] Eric Messens,[a,b] Björn Sundberg,[j] Shawn D. Mansfield,[f] John Ralph,[m] Gilles Pilate,[c] and Wout Boerjan[a,b,3]

[a] Department of Plant Systems Biology, Flanders Institute for Biotechnology, 9052 Gent, Belgium
[b] Department of Molecular Genetics, Ghent University, 9052 Gent, Belgium
[c] Unité Amélioration Génétique et Physiologie Forestières, Institut National de la Recherche Agronomique, 45166 Olivet cedex, France
[d] Unité de Chimie Biologique, Unité Mixte de Recherche 206 AgroParisTech/Institut National de la Recherche Agronomique, AgroParisTech Centre de Grignon, 78850 Thiverval-Grignon, France
[e] Institut fur Forstbotanik, Universität Göttingen, 37077 Göttingen, Germany
[f] Department of Wood Science, University of British Columbia, Vancouver, BC, Canada V6T 1Z4
[g] U.S. Dairy Forage Research Center, Agricultural Research Service, Department of Horticulture, University of Wisconsin, Madison, Wisconsin 53706
[h] Centre de Recherche sur les Macromolécules Végétales, Unité Propre de Recherche 5301, Centre National de la Recherche Scientifique, 38041 Grenoble Cedex 09, France
[i] Pôle de Biotechnologies Végétales, Unité Mixte de Recherche/Unité Propre de Service 5546, Centre National de la Recherche Scientifique, 31326 Castanet Tolosan, France
[j] Department of Forest Genetics and Plant Physiology, Swedish University of Agricultural Sciences, 90183 Umeå, Sweden
[k] Max-Planck Institute of Molecular Plant Physiology, 14476 Golm-Potsdam, Germany
[l] Centre Technique du Papier, 38044 Grenoble Cedex 9, France
[m] U.S. Dairy Forage Research Center, Agricultural Research Service, U.S. Department of Agriculture and Department of Biological Systems Engineering, University of Wisconsin, Madison, Wisconsin 53706

Cinnamoyl-CoA reductase (CCR) catalyzes the penultimate step in monolignol biosynthesis. We show that downregulation of CCR in transgenic poplar (*Populus tremula* × *Populus alba*) was associated with up to 50% reduced lignin content and an orange-brown, often patchy, coloration of the outer xylem. Thioacidolysis, nuclear magnetic resonance (NMR), immunocytochemistry of lignin epitopes, and oligolignol profiling indicated that lignin was relatively more reduced in syringyl than in guaiacyl units. The cohesion of the walls was affected, particularly at sites that are generally richer in syringyl units in wild-type poplar. Ferulic acid was incorporated into the lignin via ether bonds, as evidenced independently by thioacidolysis and by NMR. A synthetic lignin incorporating ferulic acid had a red-brown coloration, suggesting that the xylem coloration was due to the presence of ferulic acid during lignification. Elevated ferulic acid levels were also observed in the form of esters. Transcript and metabolite profiling were used as comprehensive phenotyping tools to investigate how *CCR* downregulation impacted metabolism and the biosynthesis of other cell wall polymers. Both methods suggested reduced biosynthesis and increased breakdown or remodeling of noncellulosic cell wall polymers, which was further supported by Fourier transform infrared spectroscopy and wet chemistry analysis. The reduced levels of lignin and hemicellulose were associated with an increased proportion of cellulose. Furthermore, the transcript and metabolite profiling data pointed toward a stress response induced by the altered cell wall structure. Finally, chemical pulping of wood derived from 5-year-old, field-grown transgenic lines revealed improved pulping characteristics, but growth was affected in all transgenic lines tested.

[1] These authors contributed equally to this work.
[2] Current address: Department of Forest Resources, Dongguk University, Seoul, Korea.
[3] Address correspondence to wout.boerjan@psb.ugent.be.
The author responsible for distribution of materials integral to the findings presented in this article in accordance with the policy described in the Instructions for Authors (www.plantcell.org) is: Wout Boerjan (wout.boerjan@psb.ugent.be).
[W] The online version of this article contains Web-only data.
www.plantcell.org/cgi/doi/10.1105/tpc.107.054148

INTRODUCTION

Lignins are defined as complex, heterogeneous polymers of 4-hydroxy-phenylpropanoid units (Boerjan et al., 2003; Ralph et al., 2004, 2007a). They are present mainly in the walls of secondary-thickened cells of vascular plants and represent ~20 to 30% of

the dry weight of wood. Lignins confer rigidity to the cell wall for structural support and impermeability for transport of water and nutrients over large distances. The intrinsic properties of the lignin polymers have been essential for plants to adapt to a terrestrial habitat, enabling them to grow upward, but are also crucial in determining the value of plants as raw materials. For example, lignins are a major concern for the pulp and paper industry because they need to be extracted from the wood by harsh chemical conditions to produce pure cellulose fibers (Peter et al., 2007). Similarly, they are the main limiting factor in fodder digestibility and in the conversion of plant biomass to fermentable sugars in the process to bioethanol (Chen and Dixon, 2007). Over the past decade, considerable attention has been focused on understanding the lignin biosynthetic pathway and on exploring the potential of genetic engineering to tailor lignin content and composition for industrial applications (Baucher et al., 2003; Boudet et al., 2003).

Although the roles of most genes of the monolignol pathway in determining lignin amount and composition have been elucidated, our knowledge is still scarce on how monolignol biosynthesis integrates into wider plant metabolism and how plant metabolism responds to changes in the expression of individual monolignol biosynthesis genes. With the advent of genomic tools that enable unbiased transcriptome- and metabolome-wide analyses, such interactions can now be elucidated. Indeed, deep phenotyping of transgenic plants defective in monolignol biosynthesis has revealed far-reaching consequences on gene expression in various pathways (Ranjan et al., 2004; Rohde et al., 2004; Robinson et al., 2005; Abdulrazzak et al., 2006; Shi et al., 2006; Dauwe et al., 2007). Knowledge of these broader effects at the transcriptome and metabolome levels is essential to fully comprehend the relationships between gene function and cell wall properties, how these cell wall properties are elaborated, and how they relate to the quality of raw material destined for agroindustrial processes (http://www.epobio.net/).

Cinnamoyl-CoA reductase (CCR; EC 1.2.1.44) catalyzes the conversion of feruloyl-CoA to coniferaldehyde and is considered the first enzyme in the monolignol-specific branch of the phenylpropanoid pathway (Lacombe et al., 1997). Because downregulation of the *CCR* gene in annual model plants significantly reduced lignin content (Piquemal et al., 1998; Chabannes et al., 2001a, 2001b; Jones et al., 2001; Pinçon et al., 2001; Goujon et al., 2003), downregulating *CCR* in a woody perennial was an interesting potential avenue to improve wood quality for pulping. Here, we investigated the consequences of altering *CCR* expression in transgenic poplar (*Populus tremula* × *Populus alba*) at multiple levels.

RESULTS

Generation of Transgenic Poplars Downregulated for *CCR*

Previously, we cloned a full-length *CCR* cDNA from a xylem cDNA library of poplar (*Populus trichocarpa* cv Trichobel; Leplé et al., 1998). BLAST alignments against the *P. trichocarpa* cv Nisqually 1 genome sequence (Tuskan et al., 2006) indicated the presence of a single gene model corresponding to this cDNA, whereas seven additional *CCR* homologous genes are present in the poplar genome. The *CCR* gene we cloned is the only one that is strongly expressed in developing poplar xylem (Li et al., 2005).

The poplar *CCR* cDNA sequence was used to design sense and antisense constructs under the control of the cauliflower mosaic virus (CaMV) 35S promoter for downregulation of the *CCR* expression. Following the introduction of four different constructs into poplar (*P. tremula* × *P. alba*), 40 to 60 independent transformants were regenerated for each construct. Approximately 5% of all transformants, either from sense or antisense lines, was dwarfed. These plants could be maintained for up to 7 months in tissue culture but died upon in vitro propagation and acclimation steps. The remainder of the lines had no apparent growth retardation in the greenhouse. To identify lines that were downregulated for *CCR*, all transformants were screened for the presence of an orange-brown coloration of the xylem after 3 and 7 months of growth in the greenhouse. This phenotype was previously observed in transgenic tobacco (*Nicotiana tabacum*) severely depressed for CCR activity (Piquemal et al., 1998). Based on this screen, five transgenic lines displaying the xylem coloration were identified: two (FAS13 and FAS18) and three (FS3, FS30, and FS40) lines transformed with the antisense and the sense construct, respectively (Figure 1A). RT-PCR indicated reduced steady state *CCR* transcript levels down to 3 to 4% of wild-type levels (see Supplemental Table 1 online). Four of these transgenic lines (FS3, FS30, FAS13, and FAS18) were selected in 1999 to be field-grown for up to 8 years (Figure 1D).

Variability of the Orange-Brown Phenotype

The coloration of the debarked stems of the selected greenhouse-grown transformants ranged from orange to wine-red (Figure 1A) and faded soon after peeling the bark. The color was not always uniformly distributed along the stem. Sometimes, the pattern of coloration was patchy (Figure 1B). RT-PCR revealed that *CCR* was more downregulated in the colored than in the white zones of such stems (see Supplemental Table 1 online).

For the trees grown in the field trial, the xylem coloration was consistently absent from the upper side of the branches (tension wood zone), whereas it was present on the opposite wood side (Figure 1C). Furthermore, the coloration was generally more pronounced in the basal part of the branches and the stem, whereas it became mottled and ultimately disappeared toward the apical end.

Because the intensity of the xylem coloration often varied among lines and among ramets of a given line and because the molecular phenotype correlated with the color intensity (see below), particular lines were preferred in one experiment and other lines in other experiments, depending on the xylem color intensity these trees presented at the harvest time for the different experiments. For particular experiments, red and white patches of the same stem were compared for phenotypic consequences of *CCR* downregulation.

Histochemical and Autofluorescence Changes Associated with *CCR* Downregulation

Patchy stems of 6-month-old greenhouse-grown plants and patchy branches of trees from the field trial were cross-sectioned

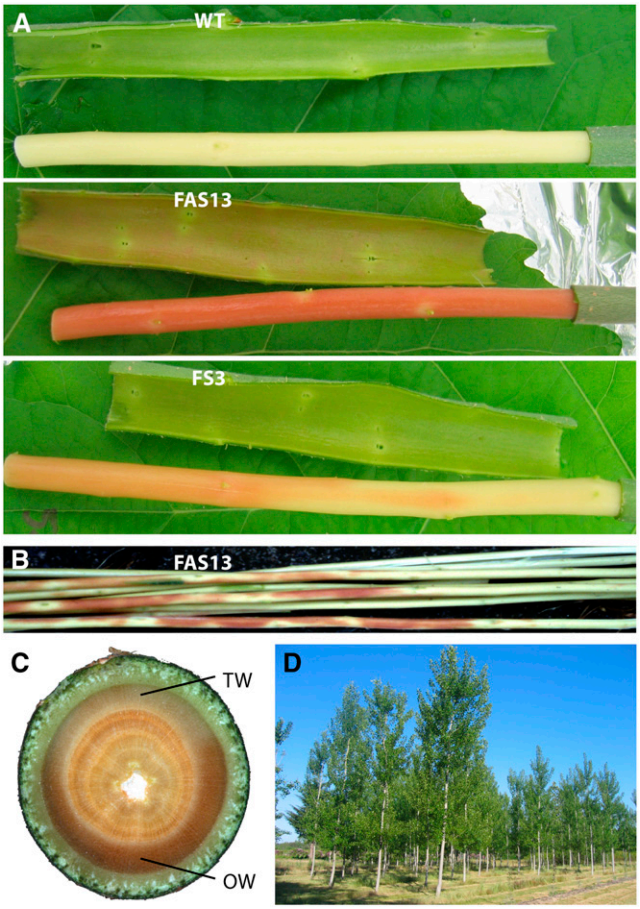

Figure 1. Phenotype of *CCR*-Downregulated Plants.

(A) Basal part of debarked stems of 4-month-old wild-type and *CCR*-downregulated poplars (FAS13 and FS3).
(B) Occasional orange-brown coloration in patches along the stem.
(C) Cross section through a branch of a 7-year-old field-grown *CCR*-downregulated poplar transformant (FAS13). The orange-brown coloration is absent in tension wood. TW, tension wood; OW, opposite wood.
(D) Field trial of *CCR*-downregulated and wild-type poplars.

and analyzed for overall morphology, altered lignification by Wiesner (phloroglucinol-HCl) and Mäule staining, altered cellulose content by Astra Blue staining, and for autofluorescence upon excitation with long-wavelength UV and blue light (Figure 2; see Supplemental Figure 1 online). Phloroglucinol-HCl and Mäule staining are considered to stain specifically cinnamaldehyde end groups (Adler et al., 1948) and syringyl (S) units in lignin (Lewis and Yamamoto, 1990), respectively. Under long-wavelength UV light, at elevated pH (pH 10.3), ferulate esters fluoresce intensely green (Harris and Hartley, 1976).

In the *CCR*-downregulated transformants, differences in histochemical staining and autofluorescence were associated with the colored areas, whereas the noncolored areas of the same sections were similar to the wild type. Specifically in the colored zones, vessels appeared irregular, and Wiesner and Mäule (data not shown) staining were weaker, whereas staining with Astra Blue was more intense (blue) in the colored areas (Figure 2B). Blue light excitation of stem sections revealed intense autofluorescence in the colored areas of *CCR*-downregulated lines (Figure 2A). This blue-excited autofluorescence was particularly intense in vessel cell walls and in the S1 layer of fibers and/or the middle lamella. Autofluorescence induced by long-wavelength UV excitation was intensely green in the colored xylem areas of the transformants, with the highest intensity in the vessels (see Supplemental Figure 1C online). Upon alkali treatment (5 N NaOH, 2 min), the green autofluorescence disappeared and autofluorescence became blue-green, similar to that of wild-type and noncolored xylem (see Supplemental Figures 1A, 1B and 1D online).

Together, these data suggest that *CCR* downregulation reduces the level of hydroxycinnamaldehydes and S units in lignin, increases the level of ferulate esters in lignin, and increases cellulose content or its accessibility by Astra Blue. Furthermore, the blue light autofluorescence in colored zones suggests the presence of metabolites or cell wall structures that are undetectable in noncolored areas.

Cell Wall Ultrastructural Morphology

Transmission electron microscopy (TEM) of cell walls stained with uranyl acetate depicts the macromolecular arrangement of the cell walls. The pattern of differential staining underscores the subdivision of the secondarily thickened walls in three sublayers, S1, S2, and S3. In poplar fibers, the S3 sublayer is generally not distinguishable. Figure 3 shows that in the colored xylem of the transformants, the inner side of the cell wall of the fibers (sublayer S2) and, more rarely, of the vessels (sublayers S2 and S3) displayed successive concentric sublayers. This stratification ranged from absent to extensive, and in some extreme cases, the cell wall appeared disorganized (Figures 3C to 3E). The disorganization was the strongest in the newly formed inner side of the cell wall, became gradually less apparent in the older layers, and was more obvious and more frequently observed in fibers than in vessels. Notably, the S1 layer of both fibers and vessels did not show any sign of altered ultrastructure. The sublayering phenotype was observed neither in the walls of neighboring colorless areas of the transformants nor in those of wild-type cells.

Patterns of Lignification in *CCR*-Downregulated Plants as Revealed by Immunogold Labeling

To examine the effects of *CCR* downregulation on lignin structure, xylem sections were immunolabeled with antibodies directed toward lignin epitopes. Dicotyledonous lignins are primarily built by the combinatorial coupling of coniferyl and sinapyl alcohol monomers with the growing polymer. This oxidative coupling gives rise to structural units with different interunit linkages, some of which can be recognized by specific antibodies. The antibodies used for topochemical visualization of lignin had been previously made against synthetic lignin generated by polymerizing coniferyl alcohol (Gzl antibody) or sinapyl alcohol (S antibody) and their specificity assessed by affinity tests (Joseleau and Ruel, 1997; Joseleau et al., 2004a, 200b). Because guaiacyl (G) polymers made from polymerizing coniferyl alcohol are enriched in condensed units involving (C–C) linkages

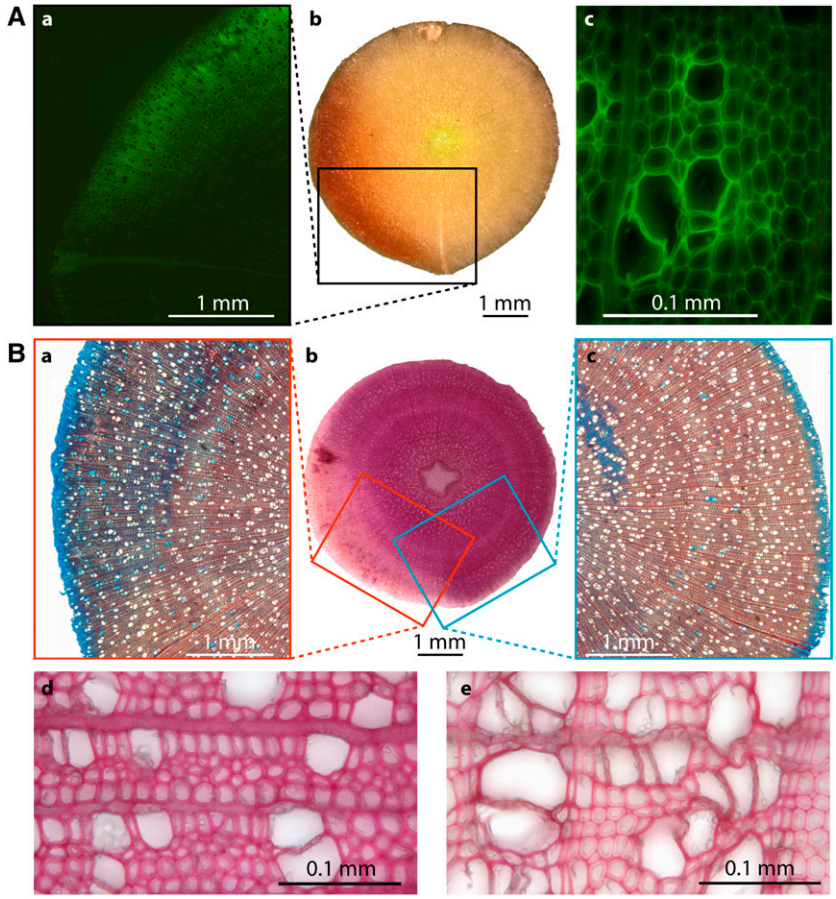

Figure 2. Histochemical Changes Associated with the Orange-Brown Xylem of *CCR*-Downregulated Poplar.

(A) Blue-excited autofluorescence of a stem section of a 6-month-old greenhouse-grown *CCR*-downregulated poplar (FAS13) with patchy orange-brown xylem coloration. Blue-excited autofluorescence (450 to 490 nm) shown for details (**[a]** and **[c]**) of the cross section **(b)**. The autofluorescence was increased preferentially in the vessels and the middle lamella and/or S1 layers of fibers in the orange-brown xylem zone. The whitish xylem areas of the transformants had no or weak blue-excited autofluorescence, reminiscent of the wild type (data not shown). Exposure time was 1 s.
(B) Astra blue and phloroglucinol staining. The cross section from **(A)** (panel **[b]**) was stained with phloroglucinol **(b)** or with both phloroglucinol and Astra Blue (**[a]** and **[c]**). **(d)** and **(e)** are cross sections through a wild-type branch **(d)** and an orange-brown zone in a FAS13 branch **(e)** from field-grown poplars, stained with phloroglucinol. Astra Blue staining was more intense, whereas phloroglucinol staining was less intense in the orange-brown zones of the transformants compared with the wild type.

and syringyl (S) polymers preferentially make noncondensed units connected by (β–O–4) linkages, immunolabeling of the cell walls with these antibodies provides insight into the local lignin structure within individual cell walls. In both wild-type and transgenic lines, S labeling was weaker in vessels than in fibers, in accordance with the lower S unit content in the lignin of vessels (Baucher et al., 1998) (Figures 3F and 3G). In fibers of wild-type plants, labeling with the S antibody revealed more abundant S epitopes in the inner part of the S2 sublayer. In the fibers of the colored areas of the FS3 line, S labeling was homogeneously distributed over the entire S2 sublayer but more weakly than that in the inner part of the S2 sublayer in wild-type fibers. The distribution pattern of the G subunits obtained with the Gzl antibody was similar between FS3 and the wild type (data not shown). In summary, *CCR* downregulation seemingly reduced the S epitopes in the S2 secondary wall sublayer of fibers and had no or limited effects on the G epitopes.

Altered Lignin Content in *CCR*-Downregulated Poplars

To analyze whether *CCR* downregulation reduces lignin content, as suggested by phloroglucinol-HCl and Mäule staining and cell wall structure analysis, branches were collected from 2-year-old field-grown poplars. Xylem fractions were scraped from the young developing xylem of the colored areas of the transgenic poplars and from the corresponding zones of wild-type plants. Acid-insoluble Klason lignin content in xylem samples from the lines FS3, FAS13, and FAS18 was significantly (probability of the least significant difference [P_{LSD}] < 0.001) reduced by 47, 23, and 8%, respectively, but not from FS30 (see Supplemental Table 2A

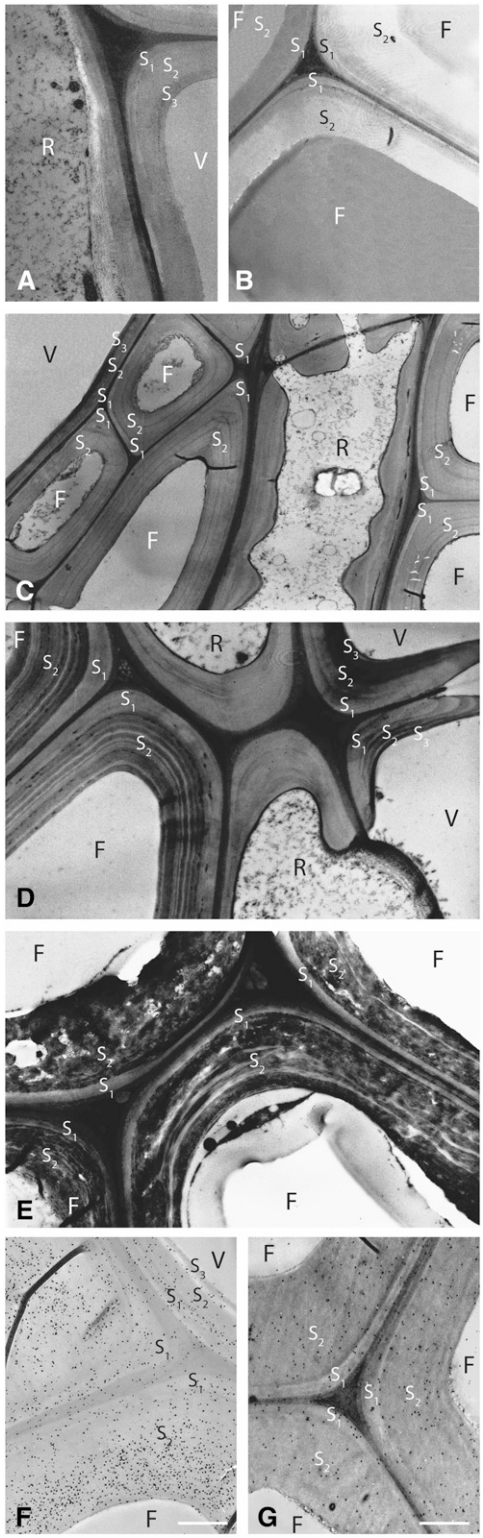

Figure 3. TEM of Xylem Sections of Wild-Type and *CCR*-Downregulated Poplars and Immunocytochemical Localization of Lignin Epitopes.

(A) and **(B)** The wild type.
(C) and **(D)** FAS18.
(E) FAS13.
(A) to **(E)** The sections are stained with uranyl acetate. Fibers and vessels of the wild type have a smooth appearance, and the layers S1 and S2 of fibers and S1, S2, and S3 of vessels are delineated (**[A]** and **[B]**). In fibers, S2 is often divided in a dark outer layer and a lighter inner layer **(B)**. In the orange-brown area of *CCR* transformants, concentric sublayers are visible in the S2 layer of fibers (**[C]** to **[E]**) and in the S2 and S3 layers of vessels **(D)**. Similar results were seen in sections of lines FS3 and FS30. The ultrastructure of the cell walls was most severely affected in the orange-brown zones of line FAS13, where the stratification was often accompanied by a loss of compactness **(E)**.
(F) and **(G)** Immunolabeling of syringyl epitopes with S antibody, performed on stem cross sections of wild-type **(F)** and FS3 **(G)** poplars, grown under controlled conditions. S epitopes concentrated in the inner part of S2 of fibers in the wild type, whereas a weaker and more homogeneous distribution of S epitopes was observed in S2 of fibers from orange-brown areas of the transformant. Note: differences in the size of gold particles are due to uneven silver enhancement that modified the diameter of the gold particles, but not their number.
F, fibers; V, vessels; R, ray cell. Bars = 1 μm.

online). In agreement, the FS3 line had the most intensely colored xylem phenotype, whereas only a light patchy phenotype was observed in the samples of FS30. Additionally, acid-insoluble Klason lignin contents were measured from noncolored and colored stem xylem areas of 1-year-old greenhouse-grown FS3 and FS40. These data indicated that the decreased lignin content was associated with the coloration (see Supplemental Tables 2 and 3 online).

Altered Lignin Structure in *CCR*-Downregulated Poplars

The lignins of the FS3 and wild-type branch xylem samples and of the FS3 and FS40 stem xylem samples, described above, were analyzed structurally by thioacidolysis (Lapierre et al., 1999). Thioacidolysis selectively cleaves the β–O–4-ether bonds in the lignin polymer. The β–O–4-linked G and S lignin subunits give rise to specific monomeric degradation products that are quantified and reflect the proportion of G and S units linked by β–O–4-ether bonds. The lignin fraction that is released by thioacidolysis is referred to as the noncondensed fraction, in contrast with the units that involve condensed bonds and are not released as monomers by thioacidolysis. The total yield (S+G) and relative proportion (S/G) of the released thioacidolysis monomers are presented in Supplemental Table 2A online. Lignins from the colored area of the FS3 branches systematically released fewer thioacidolysis S and G monomers per gram of Klason lignin than wild-type lignins ($P = 0.046$), which is indicative of a higher frequency of condensed bonds in *CCR*-downregulated lines. The S/G ratio based on thioacidolysis data did not differ significantly from that of the wild type. In addition to the main S and G monomers, lignins from the colored zone of the FS3 branches released 10- to 20-fold higher amounts of a new thioacidolysis product than the control lignins ($P < 0.001$), in which this compound was recovered only in minor amounts (see Supplemental Tables 2A and 3 online). Elucidation of its structure by electron-impact mass spectroscopy (MS) indicated that this

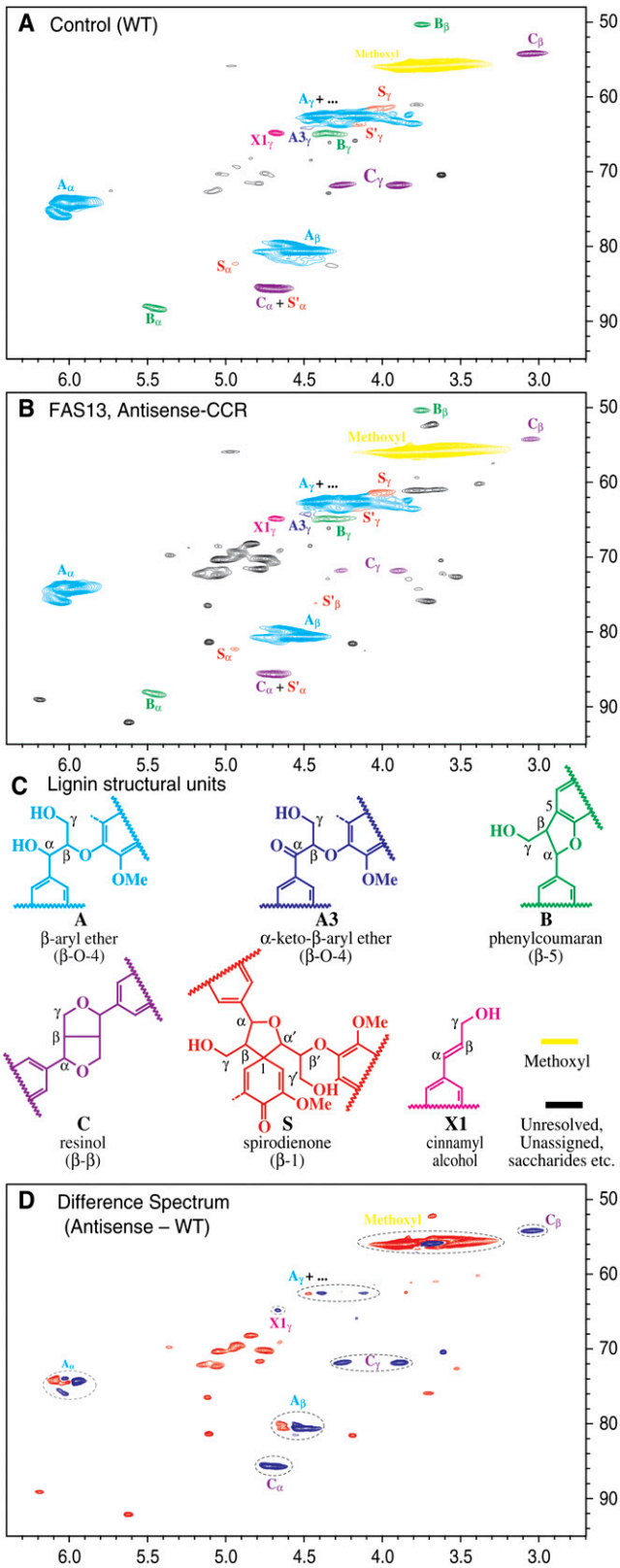

Figure 4. Side Chain Regions of HSQC Spectra from Enzyme Lignins Illustrating Lignin Structural Changes.

new product consisted of an aromatic G ring with a two-carbon side chain in which the α and β carbons are involved in a single thioether (CHR; R = SEt) and two thioethers (CHR_2), respectively. This compound was then designated as G-CHR-CHR_2. The corresponding S analog could also be observed but to a much lower extent (data not shown). Thioacidolysis released also increased amounts of ferulic acid from the FS3 colored branch samples. In the patchy stems of 1-year-old greenhouse-grown FS3 and FS40, higher amounts of the G-CHR-CHR_2 marker were released by thioacidolysis from the colored than from the non-colored areas, indicating that it was associated with the coloration. These changes in the release of thioacidolysis monomers were also confirmed in extractive-free xylem and the corresponding milled-wood extracted lignins (MWELs) of 1-year-old greenhouse-grown FS3 compared with the wild type (see Supplemental Table 2B online). In addition, analysis of the dimers released by thioacidolysis from these extractive-free xylem and MWEL fractions indicated a substantially lower yield of the syringaresinol-derived dimer (see Supplemental Table 2B online), as confirmed by nuclear magnetic resonance (NMR) analysis (see below). Furthermore, the MWEL sample of FS3 released twofold more *p*-hydroxybenzoate, vanillic acid, and ferulic acid upon alkaline hydrolysis (means ± SE based on technical replicates were 40 ± 2, 1.7 ± 0.1, and 0.6 ± 0.1 and 61 ± 0.7, 4.8 ± 1.0, and 1.5 ± 0.2 μmole/g Klason lignin in the wild type and FS3, respectively). Alkaline hydrolysis breaks mainly ester linkages. The release of ferulate is in agreement with the green autofluorescence of stem sections induced by long-wavelength UV excitation, which has been described to be caused by ferulate esters (see Supplemental Figure 1 online; Harris and Hartley, 1976).

Whereas the S/G ratio of thioacidolysis monomers reflects only the etherified units that can release monomeric products, NMR potentially measures the S/G of the entire lignin. The S/G ratio of FAS13 and FS40 lignin, calculated from NMR data, was significantly lower than that of the wild type (see Supplemental Tables 2C and 3 and Supplemental Figure 2 online). These data are supported by the interunit linkage distributions (see below).

The side chain region only peripherally reflects the changes in the S/G distribution but is rich in detail regarding the types and distribution of interunit bonding patterns present in the lignin fraction. The control lignin heteronuclear single-quantum coherence (HSQC) spectrum (Figure 4A) is typical of a guaiacyl/syringyl lignin containing some residual polysaccharides (Ralph et al., 1999). The lignin was rich in β-aryl ether units **A**, with modest amounts of phenylcoumaran **B**, and resinol **C**, and traces of spirodienone **S** units, typical for angiosperm lignins. Resinols **C** arise usually from sinapyl alcohol dimerization and hence are always significantly higher in angiosperms than in gymnosperms. Finally, the cinnamyl alcohol end groups **X1**, like the resinols **C**, arise from monomer-monomer coupling (often involving G units) and are therefore relatively minor.

(A) to **(C)** HSQC spectra from lignins isolated from the wild type **(A)** and FAS13 **(B)**. The contour colors in **(A)** and **(B)** correspond with the lignin units presented in **(C)**.

(D) Difference spectrum (FAS13 – wild type) showing, primarily, the decreased resinol **C** (negative, blue) levels.

The spectra of the lignins derived from *CCR*-deficient poplars revealed differences (Figures 4B and 4D) that were assessed from the volume integral data of the two-dimensional spectrum (see Supplemental Table 2C online). The major difference was that the resinol **C** content (β–β in Supplemental Table 2C online) was considerably lower in the FAS13 and FS40 transgenic lines, which is consistent with the lower amounts of syringaresinol released by thioacidolysis and a logical consequence of the reduced S levels documented from analysis of the aromatic regions, but the magnitude of the reduction suggests that relatively less dimerization (and more endwise coupling) occurred in the *CCR*-downregulated lines. This observation is further validated by the relatively high β-aryl ether levels in the transgenic lines (see Supplemental Table 2C online).

Elucidating the Derivation of the G-CHR-CHR_2 Thioacidolysis Compound

The G-CHR-CHR_2 thioacidolysis product could not be derived from any of the normal monolignol coupling products in the lignin polymer because the involvement of the β carbon in two thioethers revealed that this β carbon was at the oxidation level of an aldehyde. Instead, the increased incorporation of ferulic acid into the lignin, as found by thioacidolysis, suggested that G-CHR-CHR_2 was a specific coupling product of ferulic acid into the polymer. To test whether ferulic acid could produce the precursors from which the thioacidolysis marker derives during free-radical polymerization, low levels (~5%) of [8-^{13}C]-labeled ferulic acid were introduced into a 50:50 coniferyl alcohol:sinapyl alcohol synthetic lignin (dehydrogenation polymer [DHP]) with peroxidase/H_2O_2 to generate the required radicals. This DHP had the same structure as a DHP without incorporation of ferulic acid but had two small characteristic ferulic acid–derived components as seen by their $^{13}C_8$–$^1H_8$ correlations at 103.5/6.0 and 116/6.3 ppm in HSQC spectra of the acetylated DHP (see Supplemental Figure 3 online). Thioacidolysis efficiently liberated the G-CHR-CHR_2 marker compound from this synthetic DHP but not from the control DHP without ferulic acid (data not shown). In addition, HSQC correlation peaks matching those in the DHP were found at low levels in the NMR spectra of lignins isolated from transgenic poplars but not in those of the control (see Supplemental Figure 3 online). Therefore, one or both of these structures in the lignin polymer might be the source of the thioacidolysis G-CHR-CHR_2 marker compound. The ferulic acid–enriched DHP was orange-brown colored as the xylem of *CCR*-suppressed transformants, suggesting that the coloration is due to the presence of ferulic acid during lignification. A complete description of the elucidation of the marker structure and its derivation from ferulic acid–derived structures is reported elsewhere (Ralph et al., 2007b).

HPLC Analyses of Soluble Phenolics

The increased amount of ferulic acid in the lignin of *CCR*-downregulated poplars, as shown by thioacidolysis and NMR, or esterified, as indicated by alkaline hydrolysis, pointed to an increased flux through the phenylpropanoid pathway toward ferulic acid. To study this flux change, the different cinnamic acids and cinnamaldehydes present in young developing xylem, scraped from 3-month-old greenhouse-grown wild-type and *CCR*-downregulated poplars (FS3, FS40, and FAS13), were analyzed by liquid chromatography–mass spectrometry (LC-MS) with selected ion monitoring (Morreel et al., 2004b). The concentrations (mean ± SE) of ferulic acid, sinapic acid, coniferaldehyde, and sinapaldehyde were 75.5 ± 16, 197 ± 40, 28.3 ± 4, and 90.8 ± 14 pmole/mg dry weight in the wild-type poplars and 111 ± 30, 384 ± 140, 29.9 ± 12, and 77.3 ± 29 pmole/mg dry weight in the *CCR*-downregulated lines, respectively. Because of the large variation, the mean values did not significantly differ between the transgenic lines and the wild type with a nested analysis of variance (ANOVA) model. However, when the six ratios of the ion current signal of these four intermediates were analyzed by the same statistical model (Morreel et al., 2004b), all four cinnamic acid:cinnamaldehyde ratios were approximately doubled in *CCR*-downregulated lines (Table 1), indicating that the concentrations of ferulic and sinapic acids had increased relative to those of coniferaldehyde and sinapaldehyde in the *CCR*-downregulated lines.

Table 1. Mean Ratios (± SE) of the Concentrations of Phenylpropanoid Pathway Intermediates in the Xylem of Control and *CCR*-Downregulated Poplars

	Control			*CCR*-Downregulated		
Ratio	Wild Type $n = 5$	35S 17B $n = 6$	35S 21B $n = 8$	FS3 $n = 4$	FS40 $n = 4$	FAS13 $n = 6$
FA/SA	0.36 ± 0.07	0.44 ± 0.06	0.31 ± 0.06	0.44 ± 0.14	0.39 ± 0.10	0.21 ± 0.06
FA/Cal	2.44 ± 0.57	3.08 ± 0.72	2.75 ± 1.17	**7.00 ± 2.39**	**5.42 ± 2.20**	**5.31 ± 2.78**
SA/Cal	6.25 ± 1.17	5.88 ± 1.38	5.88 ± 1.04	**12.5 ± 3.1**	**10.0 ± 3.0**	**16.7 ± 5.6**
FA/Sal	0.63 ± 0.14	1.05 ± 0.20	0.80 ± 0.32	**1.82 ± 0.56**	**2.27 ± 0.81**	**2.11 ± 1.23**
SA/Sal	1.86 ± 0.25	2.49 ± 0.42	2.23 ± 0.44	**4.51 ± 1.58**	**5.29 ± 1.24**	**8.69 ± 3.45**
Cal/Sal	0.26 ± 0.01	0.36 ± 0.05	0.31 ± 0.04	0.26 ± 0.04	0.45 ± 0.09	0.37 ± 0.03

The mean ratios of the selected ion currents of the pseudomolecular ions, obtained by LC-MS atmospheric pressure chemical ionization in the negative mode, for ferulic acid (FA), sinapic acid (SA), coniferaldehyde (Cal), and sinapaldehyde (Sal) are given for the control poplars (wild-type and transgenic lines 35S 17B and 35S 21B) and *CCR*-downregulated poplars (lines FS3, FS40, and FAS13). Significantly different ratios in the *CCR*-downregulated lines relative to the control lines, revealed by applying a nested ANOVA model (Morreel et al., 2004b), are indicated in bold. Data are mean ± SE from biological replicates. *n*, number of biological replicates.

A more comprehensive picture of the flux changes through the phenylpropanoid and monolignol pathways was obtained by reversed phase HPLC-UV/Vis analysis of the methanol-soluble phenolics present in the same samples. When the heights of the 91 chromatogram peaks that could be quantified were summed and expressed relative to the dry weight, a 2.8-fold higher value was obtained in the transgenic lines, indicating prominent shifts in aromatic metabolism (data not shown). Of the 91 peaks, a nested or a one-way ANOVA model indicated that 19 differed in abundance, four of which were higher and 15 lower in abundance in the *CCR*-downregulated lines. Of the four elevated peaks, two were major peaks in *CCR*-downregulated poplars and had been previously identified as O^4-β-D-glucopyranosyl sinapic acid (GSA) and O^4-β-D-glucopyranosyl vanillic acid (GVA) in caffeoyl-CoA *O*-methyltransferase (*CCoAOMT*)–deficient poplar (Meyermans et al., 2000) (see Supplemental Table 4 online). GVA was increased by 24-fold in the *CCR*-downregulated lines, whereas GSA was found exclusively in the transgenic lines and, taking the detection limit into account, accumulated to at least 1000-fold higher levels. The abundance of the other two was too low for structural identification. Of the 15 compounds that were reduced in abundance, eight had been previously identified as oligolignols, and the remaining seven were too low in abundance to be purified but all had UV/Vis spectra indicative of oligolignols. These data indicate that *CCR* deficiency efficiently reduces the synthesis of low molecular mass monolignol-coupling products and that the flux through the phenylpropanoid pathway is shifted toward a small number of glucosylated phenolics.

Transcriptome Analysis

The phenotypes of the transgenic lines described above might merely result from an altered flux through monolignol biosynthesis. Alternatively, at least part of these phenotypes might be mediated by transcriptional changes in response to *CCR* deficiency. To reveal such phenotypic effects at the transcript level, gene expression was compared in the young developing xylem from the stems of 6-month-old greenhouse-grown wild-type poplars and transgenic lines FS3 and FS40. Two pools of xylem material were generated for each line (see Methods) and the transcriptome analyzed through an all-pairwise comparison design in duplicate (see Supplemental Figure 4 online) (Glonek and Solomon, 2004) with a 25K *Populus* (POP2) microarray (Sterky et al., 2004; www.populus.db.umu.se).

In total, 52 distinct genes were identified whose transcript levels were significantly differential in one or both transgenic lines (see Supplemental Table 5 online). In general, the effect on the transcript levels was stronger in FS3 than in FS40. Strikingly, all 49 genes for which differential transcript levels were revealed in FS40 displayed similar differential transcript levels in FS3. For 32 genes, the transcript levels were increased, whereas for 16 genes, they were decreased in the xylem of both *CCR*-downregulated lines. For only one gene, the expression was affected in an opposite way in both lines. In FS3, a decreased expression level was found for three additional genes.

Based on the annotations and the functional classification according to the public poplar EST database (POPULUSDB; www.populus.db.umu.se) (Sterky et al., 2004) and additional manual curation, 38 of the 49 common differentially expressed genes (78%) could be grouped into 10 functional categories. For the 11 remaining genes, the function of the most similar *Arabidopsis thaliana* protein was either unknown (two genes) or no significant similarity with an *Arabidopsis* protein was found (BLAST score < 100) (nine genes). The complete list of genes with their identification numbers on the microarray, annotation and functional classification, and relative transcript level is given in Supplemental Table 5 online.

Within secondary metabolism, the microarray data confirmed the downregulated expression level of the *CCR* gene. Furthermore, transcript levels of two distinct genes encoding Phe ammonia lyase (*PAL*), the enzyme channeling carbon from primary into secondary metabolism via the deamination of Phe, were elevated in the *CCR*-downregulated poplars. The ammonium liberated by the PAL reaction is reassimilated by Gln synthetase (Croteau et al., 2000). Accordingly, the expression of a Gln synthetase was increased in the transformants.

In addition, the transcript levels of three genes encoding enzymes involved in the metabolism of cell wall matrix polysaccharides (i.e., a *myo*-inositol oxygenase-like gene [*MIOX*] and a membrane-bound UDP-D-xylose 4-epimerase [*MUR4*]) were reduced in the *CCR*-downregulated lines, whereas that of a (1-4)-β-mannan endohydrolase was elevated (see Supplemental Figure 5 online). The transcript levels of two genes encoding glycosyltransferases, corresponding to the *Arabidopsis* glycosyltransferase *PARVUS* (At1g19300) (77 and 80% identity for the two poplar genes), with predicted involvement in pectin biosynthesis (Lao et al., 2003), were decreased in *CCR*-downregulated lines. These data pointed to a reduced biosynthesis and an increased breakdown or remodeling of hemicellulose and pectin.

Related to cell wall organization, the transcript levels of a putative arabinogalactan protein (AGP) and a lipid transfer protein were decreased. Furthermore, a Ser carboxypeptidase-like gene, likely involved in brassinosteroid (BR) signaling and a Leu-rich repeat receptor-like protein kinase that is similar to the *Arabidopsis* SERK2 displayed elevated transcript levels in the *CCR*-downregulated transformants.

The transcript levels of eight genes whose expression levels are typically elevated during stress situations were increased in the *CCR*-downregulated lines: four genes encoding metallothionein proteins, two genes encoding glutathione *S*-transferase (GST) (one *phi* and one *tau* class GST), a gene encoding an NADP-dependent oxidoreductase similar to ζ-crystallin (ZCr), and a gene encoding a U-box domain protein, similar to the fungal elicitor-induced protein CMPG1 of *Petroselinum crispum*. Overall, the transcriptome analysis revealed differences in the metabolism of cell wall constituents (lignin, carbohydrates, and proteins) and of stress resistance.

Metabolome Analysis

Complementary to transcript profiling, metabolome analysis can provide profound insight into the effects of gene misregulation on plant metabolism and the molecular mechanisms that provoke a phenotype. Metabolite profiles of young developing xylem of 3-month-old greenhouse-grown wild-type and *CCR*-downregulated poplars (lines FS3, FAS13, and FS40) were

obtained by gas chromatography–mass spectrometry (GC-MS) and subsequently analyzed by principal component analysis and *t* tests. Of the 802 analyzed compounds, 159 corresponded to known metabolites, of which 20 accumulated differentially in the *CCR*-downregulated lines compared with the wild type (Table 2).

The most prominent change was found for maleate levels, which were 2.4-fold higher in the FS40 line and 3.9-fold in lines FAS13 and FS3 than in the wild type. The concentrations of the Krebs cycle intermediates, fumaric and malic acids, had increased 2- to 2.5-fold and 1.6- to 3.0-fold, respectively. In addition, two other Krebs cycle intermediates (i.e., succinate and *cis*-aconitate) were moderately, but still significantly, more abundant (1.7- to 2-fold and 1.2- to 1.8-fold) because of *CCR* downregulation.

The largest fraction of differentially accumulating metabolites consisted of carbohydrates. In the transgenic poplars, glucose, mannose, galactose, and *myo*-inositol and the oligosaccharides raffinose and melezitose were all reduced to concentrations 0.5- to 0.8-fold lower than those found in the wild type, reflecting changes in central carbohydrate metabolism. In cell wall polysaccharide metabolism, the concentrations of glucuronate (GlcA) in the transgenic lines were 0.6- to 0.9-fold of those detected in the wild-type poplars, whereas concentrations of xylose and rhamnose were increased 1.8- to 2.6-fold and 1.2- to 1.4-fold, respectively, in the transgenic lines (see Supplemental Figure 5 online). Again, these data point to reduced synthesis and increased breakdown or remodeling of hemicelluloses and/or pectins, assuming that partial degradation of the nucleotide sugars is not at play.

In ascorbate metabolism, decreased levels of *myo*-inositol, GlcA, and L-gulono-1,4-lactone, a slightly lower concentration of dehydroascorbate dimer (0.8- to 1.0-fold) and 1.9- to 2.2-fold higher levels of glycerate, a possible breakdown product of ascorbate, were detected in the *CCR*-downregulated lines compared with the wild-type lines (see Supplemental Figure 5 online). Overall, the metabolome analysis revealed a substantial difference in maleate metabolism, modest shifts in carbohydrate metabolism, and a potential effect on ascorbate metabolism (Lorence et al., 2004).

Metabolite Correlation Networks

To reveal additional spots of differential regulation in the metabolism of the transformants, networks of strong correlations ($r > 0.80$) between metabolite levels were visualized for the wild type and each of the transgenic lines FS3, FS40, and FAS13 (see Supplemental Figure 6 online). In these networks, vertices and edges represent metabolites and strong correlations, respectively. Hubs are those metabolites (vertices) that are strongly

Table 2. Differentially Accumulating Metabolites in Young Developing Xylem of *CCR*-Downregulated Poplar, as Identified by GC-MS

	PCA				FAS13		FS40		FS3	
					$n = 8$		$n = 9$		$n = 14$	
	ID	PC7	PC8	PC9	P	x-Fold	P	x-Fold	P	x-Fold
Respiration										
Maleate	133003	0.37	0.55		<0.001	3.9	<0.001	2.4	<0.001	3.9
Fumarate	137001	0.31	0.32		<0.001	2.5	<0.01	2.0	<0.01	2.1
Succinate	134001				<0.010	1.7	<0.001	1.9	<0.001	2.0
Malate	149001				<0.001	3.0	<0.01	2.1	<0.05	1.6
cis-aconitate	176002				<0.001	1.8	<0.05	1.4		1.2
Sugar Metabolism										
Glucose	189002	0.25	−0.37			0.8	<0.1	0.6	<0.01	0.5
Mannose	188007			0.40		0.6		0.5		0.5
Galactose	191002			0.53		0.6		0.7	<0.01	0.4
myo-inositol	209002	0.25	−0.17			0.7		0.5		0.6
Raffinose	337002	0.27	0.22			0.8	<0.1	0.5	<0.05	0.5
Melezitose	346001					0.7	<0.1	0.6	<0.001	0.5
Ascorbic Acid Metabolism										
Glycerate	135003	0.25	0.30		<0.01	1.9	<0.01	1.9	<0.001	2.2
Gulono-1,4-lactone	192004	−0.30	−0.20		<0.05	0.7		0.6	<0.01	0.6
Dehydroascorbate	185002			0.43		0.8		1.0		0.8
Hemicellulose and Pectin Metabolism										
Rhamnose	172002	−0.33	0.25			1.2	<0.1	1.4	<0.1	1.3
Glucuronate	193004	−0.25	0.38			0.6		0.9		0.7
Xylose	166001				<0.001	1.9	<0.05	1.8	<0.001	2.6
Other										
Allantoin	189007	0.39	−0.20	0.42	<0.050	0.3	<0.1	0.5	<0.05	0.4
Norvaline	126001	−0.25	0.24			0.9		0.8		0.9
Benzoate	128003			−0.37		0.5		0.6		0.6

ID, mass spectral identifier (see Methods); PCA, principal component analysis; PC, principal component; P, significance based on *t* tests; *n*, number of biological replicates (wild type: 19 biological replicates). Projection of PC7 and PC8 into a two-dimensional plot allowed to partially separate the wild-type poplars from the transgenic poplars. A partial distinction between wild-type and transgenic poplars was also obtained by PC9. The loading factors of the compounds that contributed prominently (see Methods) to PC7, PC8, and/or PC9 are shown.

correlated to many other metabolites and, therefore, whose synthesis is strongly coregulated with the remainder of metabolism. Four compounds (i.e., mannose 6-phosphate [ID 231001], *S*-methyl-L-Cys [ID 144002], and two unknown [ID 313003 and 212004]) had many more connections in the correlation networks of the transgenic lines than in those of the wild type, indicating that their synthesis was highly coregulated with many other (primary) metabolites because of the *CCR* downregulation (see Supplemental Figure 6 and Supplemental Table 6 online). This was most prominent for mannose 6-phosphate that was not found at all in the correlation network of the wild type.

Fourier Transform Infrared Spectroscopy

Whole cell wall chemical changes induced by *CCR* downregulation were analyzed in stem sections of 6-month-old greenhouse-grown plants by Fourier transform infrared (FTIR) spectroscopy. The differences in absorbance of 15 absorption bands in the fingerprint region between 1800 and 600 cm^{-1} of the FTIR spectra (peaks 1 to 15; see Supplemental Figure 7 online) were registered in colored and noncolored areas of xylem sections of transformants (FS3, FS40, and FAS13) and in the wild type. Analyses were done with the ANOVA model 3 that takes the coloration intensity into account to distinguish differences between the poplar lines. In general, significant models were obtained for the intensities of 14 absorption bands (see Supplemental Table 8 online). In addition to data obtained from the literature, FTIR spectra of model compounds were recorded to aid the interpretation of FTIR data from the stem sections.

Cell wall carbohydrates had been previously associated with absorption bands at 1778 to 1691 cm^{-1} (1), 1397 to 1349 cm^{-1} (7), 1188 to 1145 cm^{-1} (10), and 1096 to 999 (12) (see Supplemental Table 8 online). More specifically, the absorption band (1) has been related to ester groups of carbohydrate origin, mainly xylans and pectins in poplar (see Supplemental Table 8 online). The intensity of all four absorption bands decreased with increasing coloration intensity.

FTIR absorption bands solely ascribed to aromatics in the cell wall were observed at 1691 to 1612 cm^{-1} (2), 1612 to 1554 cm^{-1} (3), and 1527 to 1486 cm^{-1} (4). Absorption band (2) is associated with carbonyl groups conjugated with aromatic rings and ferulic acid linked to lignin (see Supplemental Table 8 online). The apex of this absorption band (1652 cm^{-1}) corresponded to a peak that occurred in the spectrum recorded for free ferulic acid and not in those of four distinct ferulic acid ester references (methyl, ethyl, glucose, and galactose; data not shown). In the spectra of *CCR*-deficient transformants, as well as in those of the ferulic acid–containing DHP, the intensities of absorption bands (2) and (3) were increased, in agreement with increased ferulic acid incorporation in the wall and in the DHP, and fully correlated with the color intensity of the xylem. Absorption band (4), generally used to quantify lignin (see Supplemental Table 8 online), decreased with increasing coloration.

In summary, FTIR data of the transgenic lines indicated that the cell wall carbohydrate and, even more, lignin content decreased with increasing coloration intensity. The orange-brown color was associated completely with aromatically conjugated carbonyls.

Cell Wall Carbohydrate Analyses

Because both transcriptome and metabolome analyses indicated changes in cell wall polysaccharide metabolism in the transformants, the carbohydrate status of the cell walls in young developing xylem of the stems of 6-month-old greenhouse-grown wild-type and *CCR*-downregulated FS3 and FS40 poplars was analyzed (Table 3; see Supplemental Table 7 online). In the *CCR*-downregulated transformants, the reduced lignin content was associated with a significant decrease in hemicellulose content, whereas the cellulose content was increased. However,

Table 3. Cell Wall Carbohydrate Profile in Young Developing Xylem of 6-Month-Old Wild-Type and *CCR*-Downregulated Poplars

Characteristics	Wild Type	FS3	FS40
Biological replicates	6	5	5
Total lignin	20.65 ± 0.22	**16.75 ± 0.16**	**16.64 ± 0.18**
Acid-insoluble lignin (Klason)	17.70 ± 0.21	**14.54 ± 0.15**	**14.24 ± 0.18**
Acid-soluble lignin	2.95 ± 2.95	**2.21 ± 0.05**	**2.40 ± 0.04**
α-Cellulose	48.22 ± 0.69	**56.55 ± 0.49**	**57.07 ± 0.81**
Hemicellulose	30.72 ± 0.69	**23.19 ± 0.70**	**24.10 ± 0.44**
Arabinose	0.14 ± 0.01	0.12 ± 0.01	0.13 ± 0.01
Galactose	0.51 ± 0.01	**0.37 ± 0.01**	**0.41 ± 0.01**
Glucose	2.93 ± 0.11	**1.69 ± 0.11**	**1.91 ± 0.13**
Rhamnose	0.44 ± 0.01	**0.29 ± 0.01**	**0.31 ± 0.01**
Xylose	25.08 ± 0.68	**19.66 ± 0.61**	**20.22 ± 0.39**
Mannose	1.63 ± 0.04	**1.06 ± 0.05**	**1.11 ± 0.04**
Arabinose:mannose	0.10 ± 0.00	0.10 ± 0.00	0.10 ± 0.00
Galactose:mannose	0.30 ± 0.00	0.32 ± 0.02	**0.38 ± 0.02**
Glucose:mannose	1.78 ± 0.04	1.60 ± 0.05	1.72 ± 0.09
Rhamnose:mannose	0.27 ± 0.02	0.28 ± 0.02	0.30 ± 0.00
Xylose:mannose	15.40 ± 0.25	18.62 ± 0.71	**18.32 ± 0.58**

The mean and the SE are given. Lignin, α-cellulose, hemicellulose, and monosaccharide contents are expressed as weight percentage of dry weight cell wall material. Values that are significantly ($P < 0.05$) different from the wild type are indicated in bold.

because equal amounts of dry weight were analyzed and the cell wall polymers were measured as percentages, less lignin and hemicellulose will be mass-balanced by cellulose. Hydrolysis of the isolated hemicellulose revealed that the overall hemicellulose composition was similar in wild-type and *CCR*-downregulated poplar.

Chemical Pulping of the Different Poplar Lines

To determine how the decreased lignin and hemicellulose content would affect the kraft pulping characteristics of wood derived from *CCR*-downregulated poplars, stems of five 4-year-old, field-grown trees were pulped for each of the four transgenic lines (FS3, FS30, FAS13, and FAS18) and for the wild type. Various reaction conditions were used to determine the optimal alkali charge for delignification of the wood. Pulping characteristics were based on residual Kappa number, pulp viscosity, shives content (level of uncooked particles), and screened pulp yield.

The Kappa number, a measure of the residual lignin content in the pulp after cooking, was significantly affected by both the active alkali conditions ($P < 0.001$) and the poplar line ($P = 0.003$). As expected, a decrease in the Kappa number (improved delignification) was observed with increasing active alkali in the pulping process (see Supplemental Figure 8A online). At all active alkali charges, the Kappa number of the lines FS3 ($P_{LSD} = 0.012$) and FS30 ($P_{LSD} = 0.022$) was significantly lower than that of the wild type, whereas that of the FAS13 and FAS18 transgenic lines did not significantly differ from the wild type for any active alkali charge (see Supplemental Figure 8A online).

A high pulp viscosity, reflective of cellulose/hemicellulose degree of polymerization, is generally associated with better pulp and paper properties and is generally lower under higher alkali conditions. Pulp viscosity was significantly lower in the transgenic line FS3 than that in the wild type at all active alkali conditions ($P = 0.001$; $P_{LSD} = 0.004$) (see Supplemental Figure 8B online).

A significant effect of both the active alkali conditions ($P < 0.001$) and poplar line ($P = 0.004$) was observed for the proportion of uncooked particles that are complexes of assembled fibers. High levels of uncooked particles indicate that the chemical cooking conditions were not strong enough to totally dissolve the lignin and individualize the fibers. The percentage of uncooked particles was lower under higher alkali conditions and was significantly lower in the transgenic lines FS3 ($P_{LSD} = 0.017$) and FS30 ($P_{LSD} = 0.014$) than in the wild type for all alkali conditions (see Supplemental Figure 8C online).

Statistical analysis of the screened pulp yield indicated a significant interaction ($P = 0.002$) between the active alkali conditions and the poplar line. For line FS3, the optimal pulp yield was at 16% (or lower) active alkali, whereas the wild type and the other transformants required 18% active alkali to reach maximum pulp yields (see Supplemental Figure 8D online). One-way ANOVA revealed a significantly lower yield for line FS3 at 18% active alkali ($P = 0.04$; $P_{LSD} = 0.003$).

In summary, the optimal cooking conditions for the wild type were reached at 18% alkali charge. At 16%, the wild-type line had a much higher Kappa number and lower pulp yield than at 18% alkali. Both transgenic lines FS3 and FS30 were more easily cooked at 16% active alkali than the wild type, as revealed by their low percentage of uncooked particles. The two antisense lines FAS13 and FAS18 were not significantly different from the wild-type poplars.

Growth of *CCR*-Downregulated Poplar in the Field

As described above, downregulation of *CCR* resulted in stunted plants in 5% of the regenerants, but the lines that were selected for further experiments (FS3, FS30, FS40, FAS13, and FAS18) had an apparently normal development under greenhouse conditions. To investigate whether *CCR* downregulation impacted the growth characteristics of poplars during further development and under natural circumstances, growth parameters (i.e., the height, girth, girth increase, and volume and volume increase) were determined annually for all trees in the field trial (10 replicates for each of the lines FS3, FS30, FAS13, FAS18, and the wild type) (Figure 5). These growth parameters were subjected to a three-way ANOVA involving year, line, and block effects. A three-way interaction was noticed for girth increase, whereas for all other parameters, the full model could be reduced to model 1 that still included a significant interaction between the line and the position of the block in the field. All traits were subject to genotype $\times$ environment interaction. The P_{LSD} values mentioned below are based on the two-way ANOVA model involving the year and line as main factors.

The height of wild-type poplars increased linearly from 660 cm on average in 2001 to 960 cm on average in 2003 (Figure 5A). Across the complete duration of the field trial, the height was significantly lower in both the FAS13 ($P_{LSD} = 0.02$) and FS3 ($P_{LSD} < 0.001$) lines, which were 4 and 20% smaller than wild-type trees, respectively.

In wild-type poplars, the girth increased linearly from 150 to 270 mm between 2001 and 2003 (Figure 5B). As for height, the values for FAS3 and FAS13 were significantly different ($P_{LSD} < 0.001$) from those of the wild type, with 16 and 10% reduction, respectively.

Girth increase was determined in 2002 and 2003 and was on average 57 mm/year in the wild type (Figure 5C). All transgenic lines exhibited a growth reduction between 14 and 23%. These reductions corresponded to 45 mm/year ($P_{LSD} = 0.004$), 48 mm/year ($P_{LSD} = 0.04$), 44 mm/year ($P_{LSD} = 0.002$), and 48 mm/year ($P_{LSD} = 0.03$) for the FAS13, FAS18, FS3, and FS30 lines, respectively. Although the slope obtained for line FAS18 was quite different compared with the other lines, no significant clone by year interaction for girth increase was found.

Volume changed exponentially across years and rose from 3550 cm^3 in 2001 up to 16,300 cm^3 in 2003 in wild-type plants (Figure 5D). In the FAS13 and FS3 lines, a significantly lower volume was found ($P_{LSD} < 0.001$ for both lines) with an average reduction of 23 and 43% compared with the wild type, respectively.

In wild-type poplars, the volume increase augmented from 4300 cm^3/year in 2002 to 8400 cm^3/year in 2003 (Figure 5E). Values for this trait were significantly lower in the transgenic lines FAS13 ($P_{LSD} = 0.001$), FS3 ($P_{LSD} < 0.001$), and FS30 ($P_{LSD} = 0.04$), whose volume increase was on average 31, 51, and 29% lower,

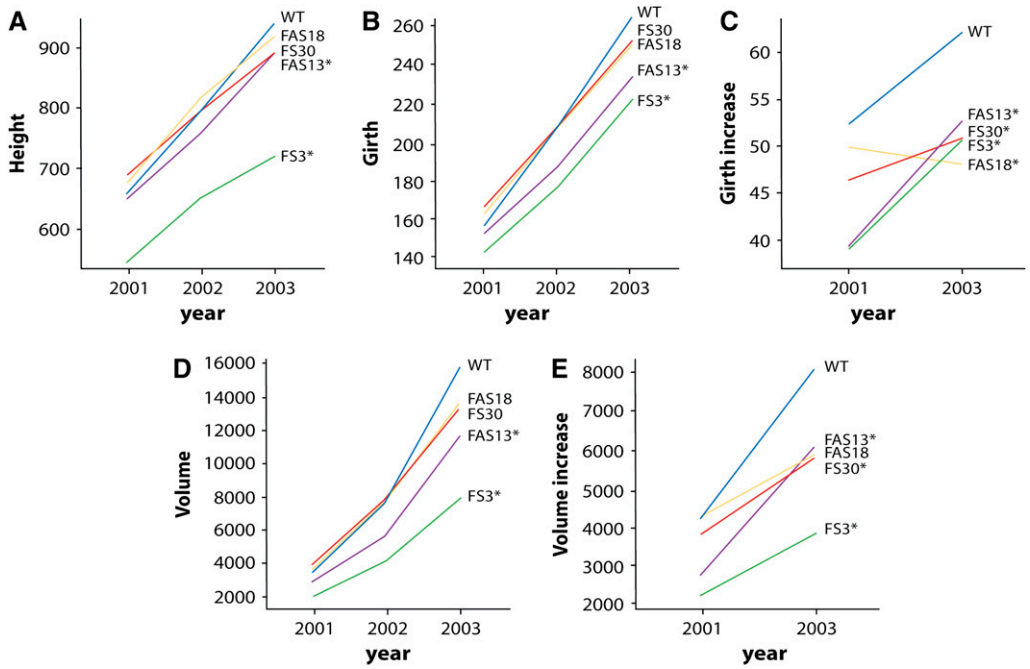

Figure 5. Growth Characteristics of Field-Grown *CCR*-Downregulated Transgenic Poplars.

For wild-type and the *CCR*-downregulated lines FS3, FS30, FAS13, and FAS18, the mean values for height **(A)**, girth **(B)**, girth increase **(C)**, volume **(D)**, and volume increase **(E)** from 2001 to 2003 are presented. Data are means of 10 biological replicates. Lines for which the given growth characteristic was significantly differential compared with the wild type are marked by an asterisk.

respectively, than in the wild type. In conclusion, all transgenic lines evaluated had reduced growth when grown in the field.

DISCUSSION

Ferulic Acid Cross-Couples with Lignin

CCR catalyzes the conversion of feruloyl-CoA to coniferaldehyde in the biosynthesis to the monolignols. Downregulation of *CCR* expression in poplar resulted in a decreased Klason lignin content and reduced abundance of a range of low molecular weight oligolignols, including dimers and trimers of monolignols (see Supplemental Table 4 online) (Morreel et al., 2004a, 2004b), which is in accordance with a decreased monolignol supply in these plants. The reduced lignin content is associated with an orange-brown coloration of the xylem. Sometimes a patchy coloration, correlated with variation in *CCR* downregulation, was observed along the stem. Patchy phenotypes associated with variation in the efficiency of gene silencing have been observed in several plants, including petunia (*Petunia hybrida*), where it was first described (Napoli et al., 1990), tobacco (Boerjan et al., 1994), and poplar (Baucher et al., 1996; Tsai et al., 1998; Meyermans et al., 2000; Pilate et al., 2002). In poplar, both developmental and environmental factors seem to contribute to the variability in phenotype (Pilate et al., 2002; this study). These phenotypic variations likely reflect the complexity of the various pathways that trigger and revert gene silencing (Fagard and Vaucheret, 2000; Kanazawa et al., 2007).

It is important to note that the variability in gene silencing can only be observed easily when downregulation of the target gene causes a visible phenotype. When no visible phenotype can be scored, such variability in gene silencing will contribute to biological variation among samples and may obscure reproducibility of phenotypic data.

Transgenic plants deficient in cinnamyl alcohol dehydrogenase (CAD) or caffeic acid 3-*O*-methyltransferase (COMT) are also typified by a reddish xylem coloration, whose origin has been attributed to the hydroxycinnamaldehydes present during polymerization (Higuchi et al., 1994; Baucher et al., 1996; Tsai et al., 1998; Kim et al., 2000). As CCR catalyzes the biosynthesis of hydroxycinnamaldehydes, the orange-brown coloration in *CCR*-downregulated plants is probably not caused by such aldehydes. Indeed, phloroglucinol staining that reacts with cinnamaldehyde end-groups in the lignin was strongly reduced in the colored zones, and structural analysis of lignins of the *CCR*-downregulated transformants indicated that the chemical determinant of the coloration is probably derived from ferulic acid. Indeed, introducing low levels (~5%) of ferulic acid into a 50:50 coniferyl alcohol:sinapyl alcohol synthetic lignin (DHP) resulted in a similar coloration of the DHP. It is also noteworthy that semi in vivo incorporation of ferulic acid into tobacco stem cross sections gave a xylem coloration that was similar to the one observed on xylem of tobacco downregulated for *CCR* (Piquemal et al., 1998).

More direct proof for the incorporation of ferulic acid into lignin was obtained from a range of experiments: thioacidolysis released the G-CHR-CHR_2 structure systematically in higher amounts from lignin of *CCR*-downregulated poplar than from wild-type lignin (see Supplemental Table 2 online), and the same thioacidolysis marker was released from the synthetic DHP including ferulic acid but not from that without ferulic acid. In addition, two-dimensional NMR spectra of the DHP showed correlation peaks (see Supplemental Figure 3B online) that are characteristic for incorporation of ferulic acid as *bis*-8–O–4-ethers and simple 4–O–β ethers (Ralph et al., 2007b) and the same correlation peaks were found at low levels in NMR spectra from lignins of the *CCR*-downregulated transformants but not in those from the wild-type lignin (see Supplemental Figure 3A online). Thioacidolysis also revealed increased amounts of simple 4–O–β-linked ferulic acid, and alkaline hydrolysis indicated an increased amount of esterified ferulic acid, as previously reported in the lignin of *CCR*-downregulated tobacco (Chabannes et al., 2001a). Further support came from FTIR, absorbances at 1691 to 1612 cm^{-1} and 1612 to 1554 cm^{-1} in FTIR spectra of the xylem of *CCR*-downregulated and wild-type trees were positively correlated with each other and with the coloration intensity, indicating an increased amount of aromatically conjugated carbonyls, such as ferulic acids with free carboxyl groups, in the lignin.

Ferulic acid incorporation does not seem to be unique to *CCR*-downregulated plants, as low levels of G-CHR-CHR_2 were also released by thioacidolysis from wild-type poplar (see Supplemental Table 2 online), as well as tobacco and *Arabidopsis*, and more substantial levels from grasses (Ralph et al., 2007a). By contrast, a recent study of the *Arabidopsis irx4* mutant, deficient in *CCR*, did not find any evidence for the incorporation of ferulic acid into lignin (Laskar et al., 2006). However, the thioacidolysis and NMR data were not presented in sufficient detail to exclude the incorporation of ferulic acid into lignin. Thus, ferulic acid appears to be incorporated into lignins, particularly in these *CCR*-deficient transgenic plants and should be considered as an authentic lignin monomer. A more in-depth chemical study of ferulic acid incorporation into lignin, the consequences on lignin structure, and a comparison with the results of Laskar et al. (2006) are presented in Ralph et al. (2007b).

Lignin Structure in *CCR*-Downregulated Poplar

The increased incorporation of ferulic acid was not the only structural change of the lignins in *CCR*-downregulated poplar. Indeed, several structural analyses illustrated a relatively stronger effect of *CCR* downregulation on S units. Thioacidolysis indicated that the lignin from the colored xylem was more condensed and yielded fewer syringaresinol-derived dimers than the wild type (see Supplemental Table 2 online). In agreement with these data, a low S/G ratio and a low frequency of resinol units was found in lignin from the *CCR*-downregulated lines by NMR (see Supplemental Table 2 online). The thioacidolysis-associated S/G ratio was not statistically different, but, as stated in the results, the latter ratio is based on the uncondensed lignin fraction only, whereas the NMR-associated S/G ratio potentially reflects the whole lignin. In addition, oligolignol profiling demonstrated that the levels of all seven oligolignols detected that involved S units were reduced, whereas the proportions of only one of the five that involved solely G units were reduced in abundance (see Supplemental Table 4 online). These chemical analytical results were supported by the immunolabeling results in TEM, showing a reduced reactivity of the cell walls of the transgenic lines with the S antibody (Figure 3), whereas no obvious variation in labeling intensity was observed with the G antibody (data not shown). The higher frequency of condensed bonds, the lower content of S units involved in β–O–4 or syringaresinol structures, and the higher degree of lignin acylation by *p*-hydroxybenzoic acid as revealed by alkaline hydrolysis of the MWEL fraction all are reminiscent of early developmental stage poplar lignin (Terashima et al., 1979). In other words, *CCR* deficiency appears to induce a delay in the lignification program as suggested for the *Arabidopsis irx4* mutant by Laskar et al. (2006), which was also characterized by a lower S/G value and a more condensed lignin.

Downregulation of *CCR* Results in the Accumulation of Phenolic Acid Glucosides

The reduced flux into the monolignol-specific branch of the phenylpropanoid pathway in the xylem of *CCR*-downregulated poplars results in the strong accumulation of GVA and GSA, of which the latter was not detected at all in wild-type poplars. Interestingly, GVA and GSA also accumulated in *CCoAOMT*-downregulated poplars, in addition to O^3-β-D-glucopyranosyl-caffeic acid (Meyermans et al., 2000; Morreel et al., 2004b). For the *CCoAOMT*-downregulated poplars, caffeoyl-CoA, the substrate of CCoAOMT, was hypothesized to be redirected to caffeic acid by a thioesterase (Guo et al., 2001). Caffeic acid would then be converted to vanillic and sinapic acid, after which all three acids would be detoxified by glucosylation (Meyermans et al., 2000). In *CCR*-downregulated poplar, O^3-β-D-glucopyranosyl-caffeic acid does not accumulate, but feruloyl-CoA, the substrate for *CCR*, might be similarly hydrolyzed to ferulic acid. Indeed, as evidenced by thioacidolysis, NMR spectra, and alkaline hydrolysis, lignin of *CCR*-downregulated poplars contains increased levels of ferulic acid. Subsequently, ferulic acid would be converted to vanillic acid and sinapic acid and further detoxified by glucosylation to GVA and GSA (Meyermans et al., 2000). The weak phloroglucinol staining of the xylem and the increased ratios of either ferulic or sinapic acid to either coniferaldehyde or sinapaldehyde in *CCR*-downregulated transformants suggest that the reduced activity of CCR results in reduced levels of coniferaldehyde and 5-hydroxyconiferaldehyde. These aldehydes have an inhibitory effect on the COMT- and ferulate-5-hydroxylase–catalyzed conversion of ferulic acid to sinapic acid (Osakabe et al., 1999; Li et al., 2000). Their reduced levels might mitigate this inhibitory effect in *CCR*-downregulated transformants, facilitating the conversion of ferulic acid to sinapic acid.

In *CCR*-downregulated tobacco, quinate conjugates of phenylpropanoid intermediates accumulated in addition to glucose conjugates (Dauwe et al., 2007). In tobacco and *Arabidopsis*, the conversion of *p*-coumaroyl-CoA to caffeoyl-CoA is thought to occur via quinate ester intermediates (Schoch et al., 2001;

Hoffmann et al., 2003), and the enzymes catalyzing this pathway might detoxify accumulating phenylpropanoid intermediates in these species. Remarkably, quinate esters were neither detected in xylem of the wild type nor in that of *CCR*-downregulated poplars, although the applied HPLC procedure readily allowed their detection in tobacco xylem (Dauwe et al., 2007). Either the quinate esters are present in concentrations below the detection limit or the hexose esters rather than the quinate esters are involved in the transesterification reactions in phenylpropanoid biosynthesis in poplar xylem. *p*-coumaroyl hexose also has a high group-transfer potential and is detectable in poplar xylem by LC-MS/MS (data not shown).

Taken together, our data indicate that downregulation of *CCR* results in a decreased flux of feruloyl-CoA to lignin and an increased flux toward ferulic acid, which is detoxified by glucosylation as GSA and GVA, or alternatively is exported to the cell wall where it is cross-coupled with lignin. The increase in ferulic acid levels might simply be the result of a reduced flux to coniferaldehyde, causing a buildup of precursors and derivatives, but possibly ferulic acid biosynthesis might also be induced as a response to a defective cell wall.

Downregulation of *CCR* Induces *PAL* Expression

The transcript levels of two *PAL* genes, encoding the enzyme that catalyzes the entry of Phe into phenylpropanoid metabolism, were increased in the *CCR*-downregulated poplar lines. One possible reason for the increased *PAL* transcript levels is that the decreased synthesis of monolignols may signal a need for increased carbon flux into this pathway. A signal for increased developmental lignification could be mediated by mechanistic aspects of the cell wall, resulting from the decreased lignin content, or by the reduced concentrations of pathway intermediates, such as cinnamaldehydes. Alternatively, the disorganization of the cell wall might induce signaling pathways that are typically induced by cell wall damage during wounding or pathogen attack and increase *PAL* expression. For example, the cellulose synthase mutant *cev1* mimics the physiological response characteristic for wounded and infected plants (Ellis et al., 2002). The closest *Arabidopsis* homolog of both induced poplar *PAL* genes is At *PAL1*, and this gene is also induced by pathogen infection and abiotic stress (Raes et al., 2003). Interestingly, in elicitor-treated cell cultures, a strong increase of PAL activity is associated with reinforcement of the cell wall by induced lignin deposition and increased amounts of wall-bound ferulic acid (Hano et al., 2006). Thus, elevated *PAL* expression is consistent with the hypothesis that ferulic acid deposition in the wall is not simply the result of sequestration of phenylpropanoid intermediates that accumulate because of suppressed CCR activity but is actively induced to strengthen the cell wall.

The suggested wound-like response induced by *CCR* deficiency is corroborated by the increased abundance of the transcript levels of scavengers of reactive oxygen species (metallothionein) (Mir et al., 2004; Wong et al., 2004) and of enzymes that detoxify oxidative stress metabolites (GSTs and ζ-crystallin-like protein) (Wilce and Parker, 1994; Dixon et al., 2002; Mano et al., 2002). Additionally, transcript levels of a gene encoding a U-box domain protein with a function in ubiquitylation were increased in the transformants, and because this protein is similar to the fungal elicitor-induced protein CMPG1 of *P. crispum*, the induced expression of this gene supports a stress response. In *CCR*-downregulated tobacco, transcript and metabolite profiling also reflected oxidative stress. In these plants, the involvement of a wound-like response in the oxidative stress was corroborated by the accumulation of feruloyl tyramine. This compound is typically elicited in solanaceous plants upon wounding or pathogen attack. Alternatively, the molecular stress response in *CCR*-downregulated tobacco was associated with photooxidative stress caused by an increased efficiency of photosystem II and a concomitantly elevated photorespiration (Dauwe et al., 2007). In the *CCR*-downregulated poplar lines, the increased transcript levels of a photosystem II reaction center protein and a Gln synthetase similarly support a possible role of photorespiratory H_2O_2 in generating an oxidative stress response.

Altered Hemicellulose and Pectin Metabolism in *CCR*-Downregulated Transformants

The differential transcriptome and metabolome in *CCR*-downregulated poplar both pointed toward increased breakdown or remodeling of noncellulosic cell wall polysaccharides (see Supplemental Figure 5 online). In poplar, the major cross-linking cell wall polysaccharides in secondary-thickened cell walls are xylan (18 to 28% of dry weight) and glucomannan (5% of dry weight) (Mellerowicz et al., 2001). The increased transcript level of (1,4)-β-mannan endohydrolase in the transformants suggests an increased breakdown of (gluco)mannan. Furthermore, xylose and rhamnose levels were increased in the transformants. Biochemically, xylose and rhamnose are only liberated during the breakdown of hemicellulose and pectin, mainly xylan and rhamnogalacturonan, respectively. Thus, the accumulation of these metabolites indicates an increased breakdown and/or remodeling of xylan and pectin. On the other hand, the differential transcriptome and metabolome indicated, in a complementary way, a decreased hemicellulose and pectin biosynthesis in the transformants (see Supplemental Figure 5 online). UDP-D-glucuronate (UDP-D-GlcA) is the precursor of most monomers of both pectin and hemicellulose. The synthesis of UDP-D-GlcA is considered rate limiting in the biosynthesis of these noncellulosic cell wall polysaccharides and can occur either via oxidation of UDP-D-glucose (UDP-D-Glc) by UDP-D-Glc dehydrogenase, which is considered to be the main pathway, or via UDP derivatization of GlcA that, in turn, is formed by oxidation of *myo*-inositol (Seitz et al., 2000). MIOX (EC 1.13.99.1) is the regulatory enzyme of the latter pathway (Kanter et al., 2005). It has been proposed that the *myo*-inositol–dependent pathway is of minor importance in maize (*Zea mays*; Kärkönen et al., 2005), yet our results support a possible in vivo role in UDP-D-GlcA production. A decreased flux through the *myo*-inositol–dependent biosynthesis pathway of UDP-D-GlcA in the *CCR*-downregulated lines was suggested by the decreased transcript levels of a *MIOX*-like gene and supported by the decreased levels of both the substrate (*myo*-inositol) and the product (GlcA) of the MIOX-catalyzed reaction. However, the differential GlcA level should be interpreted with caution as GlcA is also a cell wall polysaccharide degradation product and acts additionally as an intermediate in other

pathways, such as ascorbate biosynthesis. UDP-D-GlcA is the direct precursor of UDP-D-xylose (UDP-D-Xyl) that in itself is an important substrate for the biosynthesis of xylans and can be converted to UDP-L-arabinose by MUR4 (Burget and Reiter, 1999; Burget et al., 2003). *MUR4* transcript levels, as well as the transcript levels of two glycosyltransferases corresponding to the *Arabidopsis PARVUS* gene, were decreased in the transformants. Because UDP-L-arabinose is used by glycosyltransferases in the arabinosylation of cell wall polysaccharides, mainly the pectic rhamnogalacturonan of type I (RGI), and because a transposon-tagged *Arabidopsis parvus* mutant showed reduced levels of RGI branching (Lao et al., 2003), pectin biosynthesis might have decreased in *CCR*-downregulated transformants. The decreased expression levels of the glucosyltransferases in the *CCR*-downregulated transformants might also affect the xylan contents because the *parvus* mutant also had decreased xylan content (Lao et al., 2003).

Glucomannan is derived from the guanosine-based nucleotide sugars GDP-D-Glc and GDP-D-mannose, the latter of which originates from mannose-6-phosphate (Man-6-P). The higher transcript levels of the (1,4)-β-mannan endohydrolase suggested an increased degradation of glucomannan in the transgenic lines. In analogy with the reduced biosynthesis of xylans, it is conceivable that the biosynthesis of the glucomannans also was reduced, implying that the flux from Man-6-P toward the (gluco)mannans would be lower than in the wild type and that Man-6-P is consequently redirected toward intermediary metabolism, resulting in the tighter correlation of Man-6-P synthesis with (primary) metabolites seen in the metabolite correlation networks (see Supplemental Figure 6 online).

Thus, the combined transcriptome and metabolome analyses suggested a reduced biosynthesis and increased remodeling of hemicelluloses. Reduced hemicellulose content, accompanying the reduced lignin content in *CCR*-downregulated poplar, was indeed confirmed by wet carbohydrate analyses of the cell wall material (Table 3) and by FTIR (see Supplemental Figure 7 online).

Altered Carbohydrate Deposition Might Be Signaled through Altered Structural and Mechanical Cell Wall Properties

Similar to *PAL* induction, the modifications in the metabolism of hemicellulose and pectin might be induced in response to the lower lignin content and the associated loose structure of the walls. In *CCR*-downregulated tobacco, which shows severe structural disorders of the cell wall, alterations in hemicellulose and pectin metabolism were apparent as well (Dauwe et al., 2007). Signaling events that coordinate the deposition of the different components of the cell wall, possibly mediated by alterations in cell wall integrity, were also apparent in cellulose synthase mutants that have, besides decreased cellulose content, alterations in the deposition of hemicellulose, pectin, and lignin (Fagard et al., 2000; Ellis et al., 2002; Caño-Delgado et al., 2003).

The induction of molecular responses to stimuli, generated by altered mechanical aspects, organization, or composition of the cell wall, requires contact sites and signaling events between the cell wall and the protoplast. AGPs are proposed to be linkers between the plasma membrane and the cell wall (Kohorn, 2000) and are presumed to be involved in molecular interactions and cellular signaling between the wall and the cell (Oxley and Bacic, 1999; Showalter, 2001; Sun et al., 2004). A differentially expressed *AGP* encodes a candidate protein for signaling of the altered mechanistic aspects of the cell wall. On the other hand, a signal molecule could have mediated an altered transcription of several genes involved in cell wall carbohydrate metabolism. A possible role for BR signaling was suggested by the differential transcript levels of a SERK2-like Leu-rich repeat receptor-like protein kinase and a Ser carboxypeptidase-like protein. SERK2 has been postulated to act as a coreceptor of the BR receptor BRI1 (Albrecht et al., 2005), and the *Arabidopsis* BRI1 suppressor (BRS1) is a secreted and active Ser carboxypeptidase that is thought to be involved in an early event in the BRI1 signaling pathway (Li et al., 2001; Zhou and Li, 2005).

Altered General Carbohydrate Metabolism in *CCR*-Downregulated Transformants

An alteration in carbohydrate metabolism was revealed by the decreased amounts of glucose, mannose, and *myo*-inositol in the metabolite pools (Table 2; see Supplemental Figure 5 online). Glucose and mannose can be readily interconverted via their 6-phosphates, whereas *myo*-inositol is derived from Glc-6-P. Several *myo*-inositol–dependent pathways appear to be downregulated in the *CCR*-downregulated transformants. As mentioned above, the transcriptome and metabolome data indicated a repression of the MIOX-catalyzed conversion of *myo*-inositol into GlcA. This reaction is not only important in cell wall polysaccharide biosynthesis, for which additional data indicated a repression (see above), but is also the first step of a *myo*-inositol–dependent ascorbate biosynthetic pathway (Lorence et al., 2004). A suppression of that pathway was supported by decreased levels of gulonate-1,4-lactone, the direct precursor of ascorbate according to that pathway (see Supplemental Figure 5 online). The slightly lower concentration of the dehydroascorbate dimer in the *CCR*-downregulated transformants might reflect a decreased concentration of ascorbate. The ascorbate level itself is not reliable because ascorbate is rapidly oxidized during the extraction and derivatization procedure. On the other hand, raffinose is derived from *myo*-inositol via galactinol. Accordingly, the levels of raffinose and its breakdown product, galactose, were decreased in *CCR*-downregulated transformants.

Taken together, the decreased biosynthesis of pectin, cross-linking glycans, ascorbate, and raffinose are potentially all linked to a decrease in carbohydrate levels (glucose, mannose, and *myo*-inositol) in the primary metabolism, which, in turn, are possibly associated with a stress response. It is therefore also conceivable that the growth defects observed in the greenhouse and the field are not merely due to a disabled vascular system but additionally to the altered carbohydrate metabolism and stress response.

CCR Deficiency Results in Sublayering of the Wall

In the *CCR*-downregulated poplars, TEM microscopy revealed alternating strongly and weakly uranyl acetate-stained concentric

bands in the inner part of secondary-thickened cell walls of the colored xylem, indicating microstructural alterations between these subsequent concentric rings. This was most obvious in S2 layers of fibers, whereas this phenotype was rarer and much less pronounced in vessels.

Sublayering of the inner cell wall layers has been described before for the interfascicular fibers in *CCR1*-downregulated transgenic *Arabidopsis* (Goujon et al., 2003) and, although not stated as such, can clearly be observed on the TEM pictures of fiber and vessel walls of tobacco transformants downregulated for both *CCR* and *CAD* (Chabannes et al., 2001b). Interestingly, multilayered cell walls are not an exclusive feature of lignin-modified plants. A similar sublayering has been described in fibers of bamboo (*Bambusa* sp), banana (*Musa* sp), coconut (*Cocos nucifera*), flax (*Linum usitatissimum*), and Douglas fir (*Pseudotsuga* sp) (Esau, 1965; Mueller and Beckman, 1979; Parameswaran and Liese, 1981, 1985; Gritsch et al., 2004). In bamboo, the cellulose microfibrillar angles alternate between the subsequent layers (Parameswaran and Liese, 1980). Interestingly, association genetics in eucalyptus (*Eucalyptus* spp) has revealed that variation in cellulose microfibril angle correlates with polymorphism in the splicing of the *CCR* gene (Thumma et al., 2005). It remains to be determined whether *CCR* downregulation in transgenic poplar affects the microfibrillar angle as well.

Transgenic Trees with Improved Pulping Characteristics but Altered Growth

Wood from *CCR*-downregulated poplar is more amenable to chemical kraft pulping. Two lines are of particular interest (FS3 and FS30), because they are more easily delignified at a low alkali charge (16 versus 18%) as shown by the lower Kappa numbers and the lower levels of uncooked particles. As was observed for *CCR*-downregulated tobacco (O'Connell et al., 2002), a decrease in Kappa number is associated with *CCR* suppression. The highest level of reduction in Kappa number is found in the two lines FS3 and FS30. The initial lignin content in these transformants is lower than that in the wild type (see Supplemental Figure 8 online), which might cause a decrease in Kappa number per se, but the lower hemicellulose content might additionally be partly responsible for the lower Kappa number.

During cooking, alkali induces some polysaccharide hydrolysis; thus, viscosity values decrease when active alkali increases. The significantly lower pulp viscosity obtained for the line FS3 (at all alkali charges) indicates that cell wall polysaccharides are more easily degraded than the control. This result contrasts with previous results obtained for plants modified for their lignin metabolism and assessed for their pulping characteristics. Even in *CCR*-downregulated tobacco, viscosity values were unaffected (O'Connell et al., 2002).

For all the lines tested, differences were observed between the five blocks harvested in the field. Among the pulping characteristics, the content of uncooked particles presents the highest variation, followed by Kappa number and screened pulp yield, as determined by the mean standard deviations. The viscosity is quite homogeneous between the different clonal replicates. These variations most probably relate to variability in environmental conditions, particularly soil heterogeneity in the nursery, but also border effects or clonal variability. Clonal variability in *CCR* downregulation was indeed evident from the variability in intensity and pattern of xylem coloration between ramets (Figure 1). FS3 and FS30 are promising for pulping applications because their easier delignification might result in ~12% savings in chemicals, which means economic benefits.

In conclusion, the strongest *CCR*-downregulated transgenic poplars had several improved pulping properties, such as lower Kappa number and reduced levels of uncooked particles. Although these lines had growth penalties, *CCR* remains an interesting gene for improving wood quality for pulping. Selection of transgenic lines with an optimal, yet stable, level of downregulation will be difficult with gene silencing approaches. However, Eco-TILLING approaches might be useful in exploiting the natural variation that is still abundantly present in native poplar provenances and that has remained virtually unexploited to date. Trees harboring *CCR* alleles that result in reduced CCR activity are interesting progenitors for breeding programs. Furthermore, the lower lignin and hemicellulose levels and associated relative increase in cellulose suggest that *CCR* downregulation might be a good strategy to improve plant biomass for bioethanol production. Short-rotation coppice field trials are being established to evaluate these possibilities.

METHODS

Construction of Sense and Antisense Constructs

All DNA recombinant techniques were essentially as described (Sambrook et al., 1989). The binary vector pBIBHYG (Becker, 1990), derived from pBIN19 (Bevan, 1984), in which the neomycin phosphotransferase gene is replaced by the hygromycin phosphotransferase gene, was used to transform poplar (*Populus tremula* × *Populus alba*) with four different constructs harboring DNA sequences from a *Populus trichocarpa* cv Trichobel full-length *CCR* cDNA (accession number AJ224986), cloned in vector pBluescript SK− (Stratagene) (plasmid name: pPOPCCR2.1) (Leplé et al., 1992). This sequence shares 99% nucleotide identitity with gene model estExt_fgenesh4_kg.C_LG_III0056 of the *P. trichocarpa* cv Nisqually genome sequence (Tuskan et al., 2006). The *CCR* sequences were fused downstream from the duplicated 250-bp upstream enhancer of the CaMV 35S RNA promoter (p70) (Kay et al., 1987).

Plasmid pPOPCCR2.1 was digested by *Sma*I and *Stu*I to isolate a 1032-bp fragment carrying the coding region of the *CCR* cDNA. This fragment was cloned in the blunt-ended *Sma*I site of the vector pLBR19 that is a pUC19-derived vector containing the p70 and the CaMV terminator sequence. Two derived vectors pLBR52 and pLBR62 were obtained carrying the 1039-bp fragment either in the sense or antisense orientation, respectively. Subsequently, the *Kpn*I/*Xba*I fragments from pLBR52 and pLBR62, carrying the p70 sense or antisense insert CaMV terminator, were cloned in the *Kpn*I/*Xba*I sites of pBIBHYG, resulting in vectors pFS-*CCR* (carrying the full sense fragment) and pFAS-*CCR* (carrying the full antisense fragment).

Plasmid pPOPCCR2.1 was digested by *Bam*HI to isolate a 526-bp fragment in the 5′ end of the *CCR* cDNA. This fragment was cloned in the *Bam*HI site of pLBR19. A restriction map was used to select the clone carrying the fragment inserted into the antisense orientation. Then, the *Kpn*I/*Xba*I fragment was cloned in the *Kpn*I/*Xba*I sites of pBIBHYG, resulting in the antisense vector p5′ AS-CCR.

Plasmid pPOPCCR2.1 was digested with *Eco*RI, self-ligated, and subsequently digested by *Eco*RI and *Xho*I to isolate a 373-bp fragment

in the 3′ end of the *CCR* cDNA. This fragment was cloned in the *Eco*RI/*Sal*I sites of the pLBR19. Then, the *Kpn*I/*Xba*I fragment was cloned in the *Kpn*I/*Xba*I sites of pBIBHYG, resulting in the antisense vector p3′AS-CCR.

Poplar Transformation

The poplar clone from the Institut National de la Recherche Agronomique, number 717-1-B4 (*P. tremula* × *P. alba*), was transformed via an *Agrobacterium tumefaciens* procedure essentially as described by Leplé et al. (1992). Putative transformants were tested for their ability to root in the presence of hygromycin (20 mg/L) and screened by PCR with primers either designed for the hygromycin phosphotransferase gene or for the introduced *CCR* cDNA fragments.

Field Trial

A field trial was established in Ardon (Orléans, France) with four transgenic lines and the wild type. The transgenic lines FS3, FS30, FAS13, FAS18, and wild-type poplars were micropropagated in vitro and 10 ramets of each were acclimatized in the greenhouse in January 1999. In June 1999, upon evaluation by the French ''Commission du Génie Biomoléculaire'' (file B/FR/99.02.15) and authorization (99/023 of the 09.4.1999) from the ''Ministère de l'Agriculture,'' the 6-month-old poplar plants (1 to 1.5 meter height) were transferred to the field. Two plants for each line were planted in five different randomized blocks. Trees were planted at a 1.5 × 3 m interval. A border of control trees surrounded this area to limit environmental effects on growth and lignification. All trees were pruned at the beginning of spring 2000 to get an improved vigor of the new sprout and to homogenize the size of the plants.

Assessment of Growth Characteristics

Height and girth of the trees in the field for the years 2000 to 2003 were measured in January to February of the years 2001 to 2004, respectively. Total volume was calculated from the height and girth values [volume = (height − 100) * girth^2/12π]. Girth increase and volume increase for a given year were defined as the difference between the values for that year and the corresponding values for the previous year. Growth parameters for the year 2000 (collected in February 2001) were not included in the analysis because of the high clonal variation for growth characteristics in the first year after pruning.

Cell Wall Autofluorescence and Staining

Cross sections of stems and branches (60 or 40 μm thick) were prepared from fresh samples with either a freeze or nonfreeze microtome. Wiesner and Mäule staining reactions were essentially according to Atanassova et al. (1995). Autofluorescence was observed with a digital module R (Leica), equipped with a DFC 320 camera, a fluorescence device, and an LP515 stop filter in conjunction with a 50-W HBO mercury burner. For blue-excited autofluorescence, sections were viewed in distilled water and the excitation wavelength was 450 to 490 nm. For long-wavelength UV light–excited autofluorescence, sections were viewed at pH 10.3 (adjusted using 0.1 N NH_4Cl and 0.1 N NaOH), the excitation wavelength was 355 to 425 nm, and a long-wave pass filter at 470 nm was used.

TEM

TEM on stems of greenhouse-grown wild-type and transgenic lines (FS3, FS30, FAS13, and FAS18) was done according to Rohde et al. (2004).

Immunocytochemistry

Fourteen-week-old and 80-cm high poplars (wild type and FS3) grown under controlled conditions were used. Two internodes (10 and 16 cm) were selected for microscopic studies, and 4-mm sections were taken from the middle of the two internodes for fixation and embedded in LR White resin (Joseleau and Ruel, 1997). Specific polyclonal antibodies directed against syringyl substructures (S antibody) and homoguaiacyl substructures (Gzl antibody) were used as antisera (Joseleau and Ruel, 1997; Joseleau et al., 2004b). For TEM, samples were prepared as described (Joseleau and Ruel, 1997) and immunolabeled on ultra-thin transverse sections (500 Å) floating downward in plastic rings passed on 50-μL drops of reagents deposited on parafilm. The successive steps were as by Joseleau and Ruel (1997). The best dilutions for the antibodies were between 1/50 and 1/100, depending on the sample. Observations were made at 80 kV with a Philips CM 200 cryoelectron microscope.

All comparative immunolabeling experiments were performed in parallel to keep similar experimental conditions (dilutions of antibodies, times of contact, etc.). Preimmune serum for each antibody was assayed on the different poplar lines, under the same conditions as those for the immunogold labeling.

RT-PCR

The expression of the endogenous *CCR* gene was assessed by RT-PCR. Samples of developing xylem were collected on 2-year-old branches from 7-year-old field-grown poplars. Colored xylem was scraped from the branches of lines FS3 and FAS13, and equivalent material was harvested from wild-type poplars. Additionally, colorless xylem adjacent to colored areas was collected from the FAS13 line. Reverse transcription was performed with 2 μg of total RNA using SuperScript II according to the manufacturer's instructions (Invitrogen). The reverse transcription reaction was diluted 6 times to a final volume of 120 μL, and 5 μL was used as template for the PCR using Applied qPCR Mastermix Plus for SYBR green I (Eurogentec). PCR was performed on three biological replicates using Smart cycler (Applied Biosystems) and the standard cycling conditions. Each replicate corresponded to a pool of samples from two branches of the same tree from the field trial, harvested in June 2006. The following primer pairs were used for PCR (*CCR*, 5′CGCAAATGCTAGGGAAAGGA3′ and 5′-TTGAAACTGGATAAAGTTAGACAACCA-3′; 18S RNA, 5′-CTTCGGGATCGGAGTAATGA-3′ and 5′-GCGGAGTCCTAGAAGCAACA-3′). The raw threshold cycle (Ct) values were normalized against 18S RNA to obtain normalized ΔCt values, which were then used to calculate the difference in expression levels compared with the wild-type sample.

Lignin Analyses

Duplicate Klason lignin was determined by the standard procedure (Dence, 1992). Lignin structure was investigated with thioacidolysis as previously described (Lapierre et al., 1999). Mild alkaline hydrolysis was performed on the MWEL lignin fractions from the wild type and FS3 with 2 M NaOH, at 37°C, overnight.

Analysis of Cellulose and Hemicellulose

Wood samples harvested from 6-month-old greenhouse-grown wild-type and transgenic lines FS3 and FS40 were ground in a Wiley mill to pass a 0.4-mm screen (40 mesh) and Soxhlet extracted overnight in hot acetone to remove extractives. The wood meal was delignified with a modified version of Browning (1967) with two successive chlorite extractions by placing 200 mg of wood into 14 mL of buffer (60 mL of glacial acetic acid + 1.3 g NaOH/L) and 6 mL of 20% sodium chlorite solution ($NaClO_2$) in a 50-mL Erlenmeyer flask, capped and sealed with parafilm, and gently shaken at 50°C for 14 h. The reaction solution was decanted and the wood washed twice with 50 mL of 1% glacial acetic acid, followed by a 50-mL wash with acetone. After the first extraction, the entire

delignification procedure was repeated, and the resulting wood extract was permitted to dry in a 50°C oven overnight. A small portion of the residual (holocellulose) was tested by micro-Klason analysis (see below) to ensure that the total lignin content of each sample was below 4% (w/w).

In a 50-mL Falcon tube, 100 mg of holocellulose was extracted with 10 mL of 5% KOH for 120 min at 20°C with continuous shaking. The tubes were centrifuged at 3000*g* for 30 min at 20°C, and the supernatant was collected. The remaining pellet was washed by resuspension in 5 mL of 5% KOH by aggressive vortexing. The supernatant was isolated by centrifugation and again washed in 15 mL of water. The three supernatants (supernatant A) were pooled, while the remaining pellet was treated to the same regime with the exception of a 24% KOH solution being applied for the extractions and washes, resulting in the pooling of supernatant B. The final pellet was washed twice with 2.5 mL of acetone, washed extensively with water, allowed to dry overnight in a 50°C oven, and quantified gravimetrically, while supernatants A and B were combined. The isolated hemicellulose polysaccharides in the pooled supernatants were acidified to pH 4.0 with glacial acetic acid, precipitated with excess 95% ethanol, and collected by centrifugation.

The composition (monomer ratios) of the isolated hemicellulose was determined by HPLC (see below) after treating the hemicellulose with 1 mL of 72% H_2SO_4 at 20°C for 1 h, diluting to 4% H_2SO_4, and autoclaving at 121°C for 60 min.

Wood chemical analyses were conducted according to the micro-Klason method of Huntley et al. (2003), which is a micromodified version of the TAPPI standard. Extracted lignocellulosic material in a 15-mL vial was cooled in an ice bath, reacted with exactly 3 mL of 72% (w/w) H_2SO_4, and thoroughly mixed for 1 min. The reaction vial was immediately transferred to a water bath maintained at 20°C and mixed for 1 min every 10 min. After 2 h, the contents of each test tube were transferred to a 125-mL serum bottle with 112 mL of deionized water to rinse all residues and acids from the reaction vial. The serum bottles were sealed and autoclaved at 121°C for 60 min. Samples were allowed to cool, and the hydrolysates were vacuum-filtered through preweighed medium-coarseness sintered-glass crucibles. Each sample was washed with 200 mL of warm (~50°C) deionized water to remove residual acids and sugars and dried overnight at 105°C. The dry crucibles were reweighed to determine Klason lignin (acid-insoluble lignin) gravimetrically. The filtrate was analyzed for acid-soluble lignin by absorbance at 205 nm with a UV/Vis spectrometer (Lambda 45; Perkin-Elmer Instruments) according to the TAPPI Useful Method UM-250 (1991).

The concentration of neutral cell wall–associated carbohydrates (arabinose, rhamnose, galactose, glucose, mannose, and xylose) was determined with an HPLC system (DX-600; Dionex) equipped with an ion-exchange PA1 column, a pulsed amperometric detector with a gold electrode, and a Spectra AS50 autoinjector. Prior to injection, samples were filtered through 0.45-μm HV filters (Millipore). A 20-μL volume of sample was loaded containing fucose as an internal standard. The column was equilibrated with 250 mM NaOH and eluted with deionized water at a flow rate of 1.0 mL/min.

Phenolic Profiling

For phenolic profiling, samples of young developing xylem were harvested from stems of 3-month-old greenhouse-grown poplars. In addition to wild-type poplar, poplar transformed with a PCaMV35S-GUS construct (35S 17B and 35S 21B) (Nilsson et al., 1996; Chen et al., 2000) and transgenic poplars downregulated for *CCR* (lines FS3, FS40, and FAS13), a set of 12 transgenic poplar lines downregulated for various enzymes involved in phenylpropanoid biosynthesis (CCoAOMT, COMT, CAD, phenylcoumaran benzylic ether reductase, and COMT+CCR double transformants) were included to increase the statistical power of the experiment. Four to eight ramets were analyzed for each poplar line. In vitro propagation, growth conditions, sampling, extraction, HPLC analysis of the soluble phenolics from poplar xylem tissue, and LC-MS/MS analysis of the cinnamic acids and cinnamaldehydes were as previously described (Morreel et al., 2004a, 2004b; Damiani et al., 2005).

For the oligolignols, the shorthand naming convention was used (Morreel et al., 2004b); briefly, bold capitals for units formally derived from coniferyl alcohol (**G**), sinapyl alcohol (**S**), coniferaldehyde (**G′**), sinapaldehyde (**S′**), vanillin (**V′**), and sinapyl *p*-hydroxybenzoate (**SP**), and the interunit bond formed during the coupling reaction specified in parentheses: (8–O–4), (8–5), or (8–8).

Microarray Analyses

Ten, nine, and ten plants of the lines FS3, FS40, and the wild type, respectively, were grown for 6 months in the greenhouse. The basal 40 cm was harvested, immediately frozen in liquid nitrogen, and kept at −80°C for RNA extraction. For RNA isolation, the stems were debarked, and the developing xylem was scraped off with a razor blade. Two pools of material were generated for each line (five plants per pool). All sampled xylem tissue from line FS3 was colored. For line FS40, xylem tissue scraped from three noncolored individuals was incorporated into one of the two duplicate pools. None of the sampled plants had a patchy phenotype. The RNA isolation protocol was adapted from Chang et al. (1993). After LiCl precipitation, the RNA was resuspended in 1.8 mL 2:1 lysis buffer (RLT)/ethanol and further purified with the RNeasy mini kit (Qiagen) according to the manufacturer's recommendations. RNA concentrations and quality were assessed with an RNA 6000 Nano assay using an Agilent 2100 bioanalyzer. The RNA was stored at −80°C in 70% ethanol.

RNA was recovered by centrifugation after addition of one-tenth volume of 3 M Na-acetate, pH 5.2, and resuspended in RNase-free water. cDNA was synthesized as described (Taylor et al., 2005) with slight modifications: 30 μg of total RNA and 1 μL oligo(dT) anchor (5 μg/μL; TTTTTTTTTTTTTTTTTTTTVN) in a volume of 10 μL was incubated at 70°C for 5 min and subsequently chilled on ice. First-strand synthesis was done in reverse transcriptase buffer (Invitrogen), 0.6 μL aa-dUTP/dNTP mix (500 μM of dATP, dCTP, dGTP, 100 μM dTTP, and 400 μM aa-dUTP; Sigma-Aldrich), 1 mM DTT, 30 units of RNase inhibitor (Invitrogen), and 200 units of Superscript II RNase H− reverse transcriptase (Invitrogen) in a total volume of 30 μL. The reaction was incubated at 42°C for 3 h and terminated by addition of 10 μL 0.5 M EDTA, pH 8.0. The RNA was degraded with alkaline treatment (10 μL 1 N NaOH) during 15 min at 65°C and neutralized with 50 μL 1 M *N*-(2-hydroxyethyl)piperazine-N′-(2-ethanesulfonic acid), pH 7.0. cDNA was purified with the Qiagen QiaQuick PCR cleanup kit according to the manufacturer's instructions and eluted with 30 μL of 4 mM KPO_4, pH 8.5. Concentrations were determined spectrophotometrically with a NanoDrop ND100 (NanoDrop Technologies). Aliquots of 800 ng cDNA were dried in a speedvac (DNA SpeedVac; Thermosavant). Cy3 and Cy5 monoreactive dried dyes (GE-Healthcare) were dissolved in 120 μL 0.1 M $NaHCO_3$, pH 9.0, and 15 μL of Cy3 or Cy5 was added to 800 ng cDNA and incubated in the dark for 2 h at room temperature. Unincorporated dyes were removed with the Cyscribe GFX purification kit (GE-Healthcare) according to manufacturer's instructions, after adjustment of the volume to 50 μL with water. cDNAs for each hybridization, labeled with Cy3 and Cy5, were eluted in the same vial. Dye incorporation was evaluated spectrophotometrically with a NanoDrop ND100. The labeled cDNA was lyophilized to a volume of 82 μL.

The POP2 *Populus* glass-spotted cDNA microarrays were used for this study (http://www.populus.db.umu.se) and hybridized in an automated slide processor (Lucidea ASP Hybridization Station; Ge-Healthcare) as described by Taylor et al. (2005) according to an all pairwise-comparison design (see Supplemental Figure 2 online). A dye-swap replication was done for each hybridization. Arrays were scanned with a ScanarrayLite 4000 microarray analysis system scanner (Packard-Bell). Laser settings and photomultiplier tube were adjusted to obtain overall similar signal strength in the green and red channels and to obtain between 1 and 2% of

saturated spots. The obtained images were analyzed with Genepix Pro 5.1 (Axon Instruments). The spot diameter resize feature was set to minimum 80% and maximum 120%. The composite pixel intensity was set to 100. The median background pixel intensity was subtracted from the mean spot pixel intensity applying the local method (default option). All data were manipulated and computed with the SAS system software package for windows V8. A spot was considered good when the foreground intensity was higher than twice the background SD in both channels, or the foreground intensity was higher than four times the background SD in one channel and higher than one background SD in the other channel. From the 25,728 cDNAs spotted on the array, 24,735 were *Populus* cDNAs, of which 16,133 were expressed in at least one array. For 11,274 *Populus* cDNAs, an F-value could be calculated. For the others, the expression remained below background on most arrays.

Metabolite Profiling by GC-MS

For metabolite profiling by GC-MS, young developing xylem was sampled from stems of 3-month-old greenhouse-grown poplars as described for the phenolic analysis (Morreel et al., 2004a, 2004b). Nineteen wild-type poplars and eight, nine, and 14 poplars of the transgenic lines FAS13, FS40, and FS3, respectively, were analyzed separately. Extraction using hot methanol:chloroform:water (3:2:4 [v/v/v]) and derivatization of the polar metabolites were performed as previously described (Kaplan et al., 2004; Desbrosses et al., 2005). Ribitol, isoascorbic acid, and deuterated Ala were added as internal standards, and retention time indices determined with a C_{12}, C_{15}, C_{19}, C_{22}, C_{28}, C_{32}, and C_{36} *n*-alkane mixture. Metabolite profiling was performed according to Desbrosses et al. (2005) using a Fisons 8000 GC instrument coupled to a Fisons MD800 mass spectrometer and equipped with an AS800 autosampler and an electron impact source (ThermoQuest). In general, the GC-MS profiling protocol yielded standard deviations that are below 6% of the mean chromatogram peak abundance (Roessner et al., 2000). The quadrupole mass spectral and retention time index library (i.e., Q_MSRI) was used to integrate particular candidate mass-to-charge traces corresponding with known metabolites and with unidentified mass spectra of metabolites; the latter are referred to as mass spectral metabolite tags (Schauer et al., 2005). In total, 802 derivatized compounds were searched for in the GC-MS chromatograms, of which 159 were known metabolites. Based on the corresponding mass spectral identifiers, further information on the metabolites can be found at http://csbdb.mpimp-golm.mpg.de/csbdb/gmd/msri/gmd_smq.html. GC-MS spectral manipulation and integration were done with MassLab software version 1.4v (ThermoQuest).

Correlation Networks

Correlation networks of metabolites were constructed for the wild type, FAS13, FS40, and FS3 based on the GC-MS data from seven, eight, nine, and 14 biological replicates, respectively. Compounds that could be quantified in at least 80% of all individuals were selected for correlation analysis. After logarithmic transformation, Pearson product-moment correlation coefficients were calculated with S-plus version 6.1 (Insightful). Correlation networks were subsequently generated with the Fruchterman-Reingold three-dimensional algorithm in Pajek (http://vlado.fmf.uni-lj.si/pub/networks/pajek/).

FTIR Spectroscopy

Stems of 6-month-old greenhouse-grown wild-type, FS3, FS40, and FAS13 poplars were analyzed by FTIR spectroscopy. Attenuated total reflection spectra of reference compounds and of 30-μm-thick xylem sections were recorded with an FTIR spectrometer Equinox 55 (Bruker Optics) combined with a DuraSampl*IR* II ATR unit (Sens*IR* Europe) at a resolution of 4 cm^{-1}, 32 scans. The reference compounds analyzed were ferulic acid, methyl ferulate, ethyl ferulate, a ferulate-glucose ester (Me-6-*O*-FA-β-D-Glc), a ferulate-galactose ester (Me-6-*O*-FA-β-D-Gal), a synthetic lignin DHP made of 50:50 coniferyl:sinapyl alcohol, and a synthetic lignin DHP made of 50:50 coniferyl:sinapyl alcohol and 5% ferulic acid (Ralph et al., 2007b). Dried sections of four plants per poplar line were analyzed and, per section, spectra of three spots (1-mm diameter) were recorded. Among the 36 spots analyzed from the transgenic poplars, 12 were from noncolored, 19 from weakly colored, and five from intensely colored areas.

Spectral data were evaluated as described by Naumann et al. (2005). The spectra were vector-normalized, and peak areas were calculated by integration of the absorbance units from the baseline, over the wave number range defining the absorption band (Opus 5.5 software, method A; Bruker Optics). Fifteen absorption bands were defined and integrated: 1778 to 1691 (1), 1691 to 1612 (2), 1612 to 1554 (3), 1527 to 1486 (4), 1486 to 1442 (5), 1442 to 1397 (6), 1397 to 1349 (7), 1349 to 1293 (8), 1293 to 118 (9), 1188 to 1145 (10), 1145 to 1096 (11), 1096 to 999 (12), 999 to 917 (13), 917 to 881 (14), and 683 to 649 cm^{-1} (15).

NMR Spectroscopy

The NMR spectra were acquired on a Bruker Biospin DMX-500 instrument fitted with a cryogenically cooled 5-mm TXI $^{1}H/^{13}C/^{15}N$ gradient probe with inverse geometry (proton coils closest to the sample). Acetylated lignin preparations (60 to 80 mg) were dissolved in 0.5 mL $CDCl_3$; the central chloroform solvent peak was used as internal reference (δ_C 77.0, δ_H 7.26 ppm). The standard Bruker implementations of one-dimensional and two-dimensional (gradient-selected, ^{1}H-detected HSQC, HSQC-TOCSY, and HMBC) NMR experiments were used for structural elucidation and assignment authentication. Data for model compounds can be found in the "NMR Database of lignin and cell wall model compounds" available at http://www.dfrc.ars.usda.gov/software.html. TOCSY experiments used a 100-ms mixing time; HMBC spectra used an 80-ms long-range coupling delay. Normal HSQC experiments at 500 MHz typically had the following parameters: acquired from 8.6 to 2.4 ppm in F2 (^{1}H) with 1864 data points (acquisition time 200 ms), 158 to 40 ppm in F1 (^{13}C) with 256 increments (F1 acquisition time 8.6 ms) of 72 scans with a 1-s interscan delay, total acquisition time of 6.5 h; the d_{24} delay was set to 1.72 ms (~1/4 J). Processing used typical matched Gaussian apodization in F2 and squared sine-bell in F1. One level of linear prediction in F1 (32 coefficients) gave improved F1 resolution but was not required.

Volume integration of contours in HSQC plots was done using Bruker's TopSpin 1.3 software as described recently (Ralph et al., 2006). For quantification of S/G distributions, only the carbon-2 correlations from G units, and the carbon-2/6 correlations from S units were used, and the G integrals were logically doubled. No correction factors were necessary, except for *p*-hydroxybenzoate quantification (1.5). This response factor was determined from two-model compounds, coniferyl *p*-hydroxybenzoate, and the γ-*p*-hydroxybenzoate ester of a syringyl β-ether dimer. For quantification of the various interunit linkage types, the following well-resolved contours (see Figure 4) were integrated: **A**α, **B**α, **C**α, **S**α, and **X1**γ. Integral correction factors determined previously (Ralph et al., 2006) were used: **A**α 1.00, **B**α 0.71, and **C**α 1.06; **S**α and **X1**γ were either not or not reliably determined and were assumed as 1.00. These values were used to correct the volume integrals to provide the estimates of unit ratios in Supplemental Table 2 online.

Chemical Pulping

In February 2004, stems of the 4-year-old field-grown trees were harvested for chemical pulping analysis. For each line (FS3, FS30, FAS13, FAS18, and wild type), five stems were harvested, each derived from a distinct block from the field trial. Trees were debarked and cut into chips with a wood log chipper and screened to remove the coarse and fine elements with a chip size classifier (Lecourt et al., 2006). The kraft pulping process

(Gullichsen and Fogelholm, 2000) was simulated at laboratory scale on 200 g of oven-dried wood chips in small pressurized reactors in a rotating oil-thermostatic bath under the following conditions: active alkali = 16 to 20%, sulfidity = 25%, liquor/wood ratio = 4, temperature rise to 170°C over 90 min, and maintained for 1 h for cooking. Pulps were washed and screened on a 150-μm slotted screen to determine uncooked particles and pulp yield. Kappa number and pulp viscosity were determined according to international standards (NF ISO 302 and ISO 5351-1).

Statistical Analyses of the Data

All statistical methods are presented in the Supplemental Methods online.

Microarray Data Deposition

Data have been deposited in the UPSC-BASE *Populus* transcriptomics online (http://www.upscbase.db.umu.se/) (Sjödin et al., 2006) under experiment number 0015.

Accession Number

Sequence data from this article can be found in the GenBank/EMBL database under accession number AJ224986 (*P. trichocarpa* cv Trichobel full-length *CCR* cDNA).

Supplemental data

The following materials are available in the online version of this article.

Supplemental Figure 1. Long-Wavelength UV-Excited Autofluorescence.

Supplemental Figure 2. Aromatic Regions of HSQC Spectra from MWEL Illustrating Compositional Changes.

Supplemental Figure 3. Partial HSQC NMR Spectra.

Supplemental Figure 4. Microarray Design.

Supplemental Figure 5. Ascorbate, Hemicellulose, and Pectin Metabolism.

Supplemental Figure 6. Metabolite Correlation Networks.

Supplemental Figure 7. FTIR Spectra Overlay.

Supplemental Figure 8. Chemical Pulping Characteristics.

Supplemental Table 1. *CCR* Transcript Abundances.

Supplemental Table 2. Lignin Profile in Young Developing Xylem.

Supplemental Table 3. Statistical Analysis of Lignin Characteristics.

Supplemental Table 4. Concentration of Phenylpropanoids.

Supplemental Table 5. Identity, Expression, and Functional Classification of the Genes.

Supplemental Table 6. Number of Vertices and Edges in Correlation Networks.

Supplemental Table 7. Carbohydrate Analyses Raw Data.

Supplemental Table 8. FTIR Analysis.

Supplemental Methods.

ACKNOWLEDGMENTS

We thank Mark Van Montagu and Dirk Inzé for support, the technical staff that managed the field trial, Frédéric Légée for Klason lignin determination, Nadège Millet and Bart Ivens for in vitro culture work and plant care, Françoise Laurans and Alain Moreau for histochemical work, Marie-Claude Lesage-Descauses for quantitative PCR analysis, Isabelle Paintrand for skillful assistance with the light microscopy, Jørgen Holst Christensen for helpful discussions, Lise Jouanin for providing the pLBR19 vector, and Martine De Cock for help with the manuscript. This work was conducted in the framework of the European Union Research Program TIMBER (FAIR-CT-95-0424), EDEN (QLK5-CT-2001-00443), and COPOL (QLK5-CT-2000-01493); partial funding to H.K. and J.R. was from the U.S. Department of Energy, Energy Biosciences Program (DE-AI02-00ER15067).

Received July 11, 2007; revised October 12, 2007; accepted October 19, 2007; published November 16, 2007.

REFERENCES

Abdulrazzak, N., et al. (2006). A *coumaroyl-ester-3-hydroxylase* insertion mutant reveals the existence of nonredundant *meta*-hydroxylation pathways and essential roles for phenolic precursors in cell expansion and plant growth. Plant Physiol. **140:** 30–48. Erratum. Plant Physiol. **141:** 1708.

Adler, E., Bjorkquist, K.J., and Haggroth, S. (1948). Über die Ursache der Farbreaktionen des Holzes. Acta Chem. Scand. A **2:** 93–94.

Albrecht, C., Russinova, E., Hecht, V., Baaijens, E., and de Vries, S. (2005). The *Arabidopsis thaliana* SOMATIC EMBRYOGENESIS RECEPTOR-LIKE KINASES1 and 2 control male sporogenesis. Plant Cell **17:** 3337–3349.

Atanassova, R., Favet, N., Martz, F., Chabbert, B., Tollier, M.T., Monties, B., Fritig, B., and Legrand, M. (1995). Altered lignin composition in transgenic tobacco expressing *O*-methyltransferase sequences in sense and antisense orientation. Plant J. **8:** 465–477.

Baucher, M., Chabbert, B., Pilate, G., Van Doorsselaere, J., Tollier, M.-T., Petit-Conil, M., Cornu, D., Monties, B., Van Montagu, M., Inzé, D., Jouanin, L., and Boerjan, W. (1996). Red xylem and higher lignin extractability by down-regulating a cinnamyl alcohol dehydrogenase in poplar. Plant Physiol. **112:** 1479–1490.

Baucher, M., Monties, B., Van Montagu, M., and Boerjan, W. (1998). Biosynthesis and genetic engineering of lignin. Crit. Rev. Plant Sci. **17:** 125–197.

Baucher, M., Petit-Conil, M., and Boerjan, W. (2003). Lignin: Genetic engineering and impact on pulping. Crit. Rev. Biochem. Mol. Biol. **38:** 305–350.

Becker, D. (1990). Binary vectors which allow the exchange of plant selectable markers and reporter genes. Nucleic Acids Res. **18:** 203.

Bevan, M. (1984). Binary *Agrobacterium* vectors for plant transformation. Nucleic Acids Res. **12:** 8711–8721.

Boerjan, W., Bauw, G., Van Montagu, M., and Inzé, D. (1994). Distinct phenotypes generated by overexpression and suppression of S-adenosyl-L-methionine synthetase reveal developmental patterns of gene silencing in tobacco. Plant Cell **6:** 1401–1414.

Boerjan, W., Ralph, J., and Baucher, M. (2003). Lignin biosynthesis. Annu. Rev. Plant Biol. **54:** 519–546.

Boudet, A.M., Kajita, S., Grima-Pettenati, J., and Goffner, D. (2003). Lignins and lignocellulosics: A better control of synthesis for new and improved uses. Trends Plant Sci. **8:** 576–581.

Browning, B.L. (1967). Methods of Wood Chemistry, Vol. 2. (New York: Interscience).

Burget, E.G., and Reiter, W.-D. (1999). The *mur4* mutant of Arabidopsis is partially defective in the de novo synthesis of uridine diphospho L-arabinose. Plant Physiol. **121:** 383–389.

Burget, E.G., Verma, R., Mølhøj, M., and Reiter, W.-D. (2003). The biosynthesis of L-arabinose in plants: Molecular cloning and characterization of a Golgi-localized UDP-D-xylose 4-epimerase encoded by the *MUR4* gene of Arabidopsis. Plant Cell **15:** 523–531.

Caño-Delgado, A., Penfield, S., Smith, C., Catley, M., and Bevan, M. (2003). Reduced cellulose synthesis invokes lignification and defense responses in *Arabidopsis thaliana.* Plant J. **34:** 351–362.

Chabannes, M., Barakate, A., Lapierre, C., Marita, J.M., Ralph, J., Pean, M., Danoun, S., Halpin, C., Grima-Pettenati, J., and Boudet, A.M. (2001b). Strong decrease in lignin content without significant alteration of plant development is induced by simultaneous down-regulation of cinnamoyl CoA reductase (CCR) and cinnamyl alcohol dehydrogenase (CAD) in tobacco plants. Plant J. **28:** 257–270.

Chabannes, M., Ruel, K., Yoshinaga, A., Chabbert, B., Jauneau, A., Joseleau, J.-P., and Boudet, A.-M. (2001a). *In situ* analysis of lignins in transgenic tobacco reveals a differential impact of individual transformations on the spatial patterns of lignin deposition at the cellular and subcellular levels. Plant J. **28:** 271–282.

Chang, S., Puryear, J., and Cairney, J. (1993). A simple and efficient method for isolating RNA from pine trees. Plant Mol. Biol. Rep. **11:** 113–116.

Chen, C., Meyermans, H., Burggraeve, B., De Rycke, R.M., Inoue, K., De Vleesschauwer, V., Steenackers, M., Van Montagu, M.C., Engler, G.J., and Boerjan, W.A. (2000). Cell-specific and conditional expression of caffeoyl-CoA *O*-methyltransferase in poplar. Plant Physiol. **123:** 853–867.

Chen, F., and Dixon, R.A. (2007). Lignin modification improves fermentable sugar yields for biofuel production. Nat. Biotechnol. **27:** 759–761.

Croteau, R., Kutchan, T.M., and Lewis, N.G. (2000). Natural products (secondary metabolites). In Biochemistry and Molecular Biology of Plants, B.B. Buchanan, W. Gruissem, and R.L. Jones, eds. (Rockville, MD: American Society of Plant Physiologists), pp. 1250–1318.

Damiani, I., Morreel, K., Danoun, S., Goeminne, G., Yahiaoui, N., Marque, C., Kopka, J., Messens, E., Goffner, D., Boerjan, W., Boudet, A.M., and Rochange, S. (2005). Metabolite profiling reveals a role for atypical cinnamyl alcohol dehydrogenase CAD1 in the synthesis of coniferyl alcohol in tobacco xylem. Plant Mol. Biol. **59:** 753–769.

Dauwe, R., et al. (2007). Molecular phenotyping of lignin-modified tobacco reveals associated changes in cell wall metabolism, primary metabolism, stress metabolism and photorespiration. Plant J. **52:** 263–285.

Dence, C.W. (1992). Lignin determination. In Methods in Lignin Chemistry, Springer Series in Wood Science, S.Y. Lin and C.W. Dence, eds (Berlin: Springer-Verlag), pp. 33–61.

Desbrosses, G.G., Kopka, J., and Udvardi, M.K. (2005). *Lotus japonicus* metabolic profiling. Development of gas chromatography-mass spectrometry resources for the study of plant-microbe interactions. Plant Physiol. **137:** 1302–1318.

Dixon, D.P., Lapthorn, A., and Edwards, R. (2002). Plant glutathione transferases. Genome Biol. **3:** reviews3004.1–3004.10.

Ellis, C., Karafyllidis, I., Wasternack, C., and Turner, J.G. (2002). The Arabidopsis mutant *cev1* links cell wall signaling to jasmonate and ethylene responses. Plant Cell **14:** 1557–1566.

Esau, K. (1965). Plant Anatomy, 2nd ed. (New York: John Wiley & Sons).

Fagard, M., Desnos, T., Desprez, T., Goubet, F., Refregier, G., Mouille, G., McCann, M., Rayon, C., Vernhettes, S., and Höfte, H. (2000). *PROCUSTE1* encodes a cellulose synthase required for normal cell elongation specifically in roots and dark-grown hypocotyls of Arabidopsis. Plant Cell **12:** 2409–2424.

Fagard, M., and Vaucheret, H. (2000). (Trans)gene silencing in plants: How many mechanisms. Annu. Rev. Plant Physiol. Plant Mol. Biol. **51:** 167–194.

Glonek, G.F.V., and Solomon, P.J. (2004). Factorial and time course designs for cDNA microarray experiments. Biostatistics **5:** 89–111.

Goujon, T., Ferret, V., Mila, I., Pollet, B., Ruel, K., Burlat, V., Joseleau, J.-P., Barrière, Y., Lapierre, C., and Jouanin, L. (2003). Down-regulation of the *AtCCR1* gene in *Arabidopsis thaliana*: Effects on phenotype, lignins and cell wall degradability. Planta **217:** 218–228.

Gritsch, C.S., Kleist, G., and Murphy, R.J. (2004). Developmental changes in cell wall structure of phloem fibres of the bamboo *Dendrocalamus asper.* Ann. Bot. (Lond.) **94:** 497–505.

Gullichsen, J., and Fogelholm, C.-J. (2000). Chemical Pulping, Paper Making Science and Technology, Vol. 6. (Helsinki, Finland: Tappi Press).

Guo, D., Chen, F., Inoue, K., Blount, J.W., and Dixon, R.A. (2001). Downregulation of caffeic acid 3-*O*-methyltransferase and caffeoyl CoA 3-*O*-methyltransferase in transgenic alfalfa: Impacts on lignin structure and implications for the biosynthesis of G and S lignin. Plant Cell **13:** 73–88.

Hano, C., Addi, M., Bensaddek, L., Crônier, D., Baltora-Rosset, S., Doussot, J., Maury, S., Mesnard, F., Chabbert, B., Hawkins, S., Lainé, E., and Lamblin, F. (2006). Differential accumulation of monolignol-derived compounds in elicited flax (*Linum usitatissimum*) cell suspension cultures. Planta **223:** 975–989.

Harris, P.J., and Hartley, R.D. (1976). Detection of bound ferulic acid in cell walls of the Gramineae by ultraviolet fluorescence microscopy. Nature **259:** 508–510.

Higuchi, T., Ito, T., Umezawa, T., Hibino, T., and Shibata, D. (1994). Red-brown color of lignified tissues of transgenic plants with antisense CAD gene: Wine-red lignin from coniferyl aldehyde. J. Biotechnol. **37:** 151–158.

Hoffmann, L., Maury, S., Martz, F., Geoffroy, P., and Legrand, M. (2003). Purification, cloning and properties of an acyltransferase controlling shikimate and quinate ester intermediates in phenylpropanoid metabolism. J. Biol. Chem. **278:** 95–103.

Huntley, S.K., Ellis, D., Gilbert, M., Chapple, C., and Mansfield, S.D. (2003). Significant increases in pulping efficiency in C4H–F5H-transformed poplars: Improved chemical savings and reduced environmental toxins. J. Agric. Food Chem. **51:** 6178–6183.

Jones, L., Ennos, A.R., and Turner, S.R. (2001). Cloning and characterization of *irregular xylem4* (*irx4*): A severely lignin-deficient mutant of *Arabidopsis.* Plant J. **26:** 205–216.

Joseleau, J.-P., Faix, O., Kuroda, K.-I., and Ruel, K. (2004b). A polyclonal antibody directed against syringylpropane epitopes of native lignins. C. R. Biol. **327:** 809–815.

Joseleau, J.-P., Imai, T., Kuroda, K., and Ruel, K. (2004a). Detection in situ and characterization of lignin in the *G*-layer of tension wood fibres of *Populus deltoides.* Planta **219:** 338–345.

Joseleau, J.-P., and Ruel, K. (1997). Study of lignification by noninvasive techniques in growing maize internodes. An investigation by Fourier transform infrared cross-polarization-magic angle spinning ^{13}C-nuclear magnetic resonance spectroscopy and immunocytochemical transmission electron microscopy. Plant Physiol. **114:** 1123–1133.

Kanazawa, A., O'Dell, M., and Hellens, R.P. (2007). Epigenetic inactivation of chalcone synthase-A transgene transcription in petunia leads to a reversion of the post-transcriptional gene silencing phenotype. Plant Cell Physiol. **48:** 638–647.

Kanter, U., Usadel, B., Guerineau, F., Li, Y., Pauly, M., and Tenhaken, R. (2005). The inositol oxygenase gene family of *Arabidopsis* is involved in the biosynthesis of nucleotide sugar precursors for cell-wall matrix polysaccharides. Planta **221:** 243–254.

Kaplan, F., Kopka, J., Haskell, D.W., Zhao, W., Schiller, K.C., Gatzke, N., Sung, D.Y., and Guy, C.L. (2004). Exploring the temperature-stress metabolome of Arabidopsis. Plant Physiol. **136:** 4159–4168.

Kärkönen, A., Murigneux, A., Martinant, J.-P., Pepey, E., Tatout, C., Dudley, B.J., and Fry, S.C. (2005). UDP-glucose dehydrogenases of maize: A role in cell wall pentose biosynthesis. Biochem. J. **391:** 409–415.

Kay, R., Chan, A., Daly, M., and McPherson, J. (1987). Duplication of CaMV 35*S* promoter sequences creates a strong enhancer for plant genes. Science **236:** 1299–1302.

Kim, H., Ralph, J., Yahiaoui, N., Pean, M., and Boudet, A.-M. (2000). Cross-coupling of hydroxycinnamyl aldehydes into lignins. Org. Lett. **2:** 2197–2200.

Kohorn, B.D. (2000). Plasma membrane-cell wall contacts. Plant Physiol. **124:** 31–38.

Lacombe, E., Hawkins, S., Van Doorsselaere, J., Piquemal, J., Goffner, D., Poeydomenge, O., Boudet, A.-M., and Grima-Pettenati, J. (1997). Cinnamoyl CoA reductase, the first committed enzyme of the lignin branch biosynthetic pathway: Cloning, expression and phylogenetic relationships. Plant J. **11:** 429–441.

Lao, N.T., Long, D., Kiang, S., Coupland, G., Shoue, D.A., Carpita, N.C., and Kavanagh, T.A. (2003). Mutation of a family 8 glycosyltransferase gene alters cell wall carbohydrate composition and causes a humidity-sensitive semi-sterile dwarf phenotype in *Arabidopsis.* Plant Mol. Biol. **53:** 687–701.

Lapierre, C., Pollet, B., Petit-Conil, M., Toval, G., Romero, J., Pilate, G., Leplé, J.-C., Boerjan, W., Ferret, V., De Nadai, V., and Jouanin, L. (1999). Structural alterations of lignins in transgenic poplars with depressed cinnamyl alcohol dehydrogenase or caffeic acid *O*-methyltransferase activity have opposite impact on the efficiency of industrial kraft pulping. Plant Physiol. **119:** 153–163.

Laskar, D.D., Jourdes, M., Patten, A.M., Helms, G.L., Davin, L.B., and Lewis, N.G. (2006). The Arabidopsis cinnamoyl CoA reductase *irx4* mutant has a delayed but coherent (normal) program of lignification. Plant J. **48:** 674–686.

Lecourt, M., Petit-Conil, M., and Nougier, P. (2006). Potential of various species to produce thermomechanical pulp. Assoc. Tech. Ind. Papet. **60:** 20–25.

Leplé, J.C., Brasileiro, A.C.M., Michel, M.F., Delmotte, F., and Jouanin, L. (1992). Transgenic poplars: Expression of chimeric genes using four different constructs. Plant Cell Rep. **11:** 137–141.

Leplé, J.-C., Grima-Pettenati, J., Van Montagu, M., and Boerjan, W. (1998). A cDNA encoding cinnamoyl-CoA reductase from *Populus trichocarpa* (Accession No. AJ224986) (PGR98-121). Plant Physiol. **117:** 1126.

Lewis, N.G., and Yamamoto, E. (1990). Lignin: Occurrence, biogenesis, and biodegradation. Annu. Rev. Plant Physiol. Plant Mol. Biol. **41:** 455–496.

Li, J., Lease, K.A., Tax, F.E., and Walker, J.C. (2001). BRS1, a serine carboxypeptidase, regulates BRI1 signaling in *Arabidopsis thaliana.* Proc. Natl. Acad. Sci. USA **98:** 5916–5921.

Li, L., Cheng, X., Lu, S., Nakatsubo, T., Umezawa, T., and Chiang, V.L. (2005). Clarification of cinnamoyl co-enzyme A reductase catalysis in monolignol biosynthesis of aspen. Plant Cell Physiol. **46:** 1073–1082.

Li, L., Popko, J.L., Umezawa, T., and Chiang, V.L. (2000). 5-Hydroxyconiferyl aldehyde modulates enzymatic methylation for syringyl monolignol formation, a new view of monolignol biosynthesis in angiosperms. J. Biol. Chem. **275:** 6537–6545.

Lorence, A., Chevone, B.I., Mendes, P., and Nessler, C.L. (2004). *myo*-Inositol oxygenase offers a possible entry point into plant ascorbate biosynthesis. Plant Physiol. **134:** 1200–1205.

Mano, J., Torii, Y., Hayashi, S.-i., Takimoto, K., Matsui, K., Nakamura, K., Inzé, D., Babiychuk, E., Kushnir, S., and Asada, K. (2002). The NADPH:quinone oxidoreductase P1-ζ-crystallin in *Arabidopsis* catalyzes the α,β-hydrogenation of 2-alkenals: Detoxication of the lipid peroxide-derived reactive aldehydes. Plant Cell Physiol. **43:** 1445–1455.

Mellerowicz, E.J., Baucher, M., Sundberg, B., and Boerjan, W. (2001). Unravelling cell wall formation in the woody dicot stem. Plant Mol. Biol. **47:** 239–247.

Meyermans, H., et al. (2000). Modification in lignin and accumulation of phenolic glucosides in poplar xylem upon down-regulation of caffeoyl-coenzyme A *O*-methyltransferase, an enzyme involved in lignin biosynthesis. J. Biol. Chem. **275:** 36899–36909.

Mir, G., Domènech, J., Huguet, G., Guo, W.-J., Goldsbrough, P., Atrian, S., and Molinas, M. (2004). A plant type 2 metallothionein (MT) from cork tissue responds to oxidative stress. J. Exp. Bot. **55:** 2483–2493.

Morreel, K., Ralph, J., Kim, H., Lu, F., Goeminne, G., Ralph, S., Messens, E., and Boerjan, W. (2004a). Profiling of oligolignols reveals monolignol coupling conditions in lignifying poplar xylem. Plant Physiol. **136:** 3537–3549.

Morreel, K., Ralph, J., Lu, F., Goeminne, G., Busson, R., Herdewijn, P., Goeman, J.L., Van der Eycken, J., Boerjan, W., and Messens, E. (2004b). Phenolic profiling of caffeic acid *O*-methyltransferase-deficient poplar reveals novel benzodioxane oligolignols. Plant Physiol. **136:** 4023–4036.

Mueller, W.C., and Beckman, C.H. (1979). Isotropic layers in the secondary cell walls of fibers in the roots of banana and other monocotyledons. Can. J. Bot. **57:** 2776–2781.

Napoli, C., Lemieux, C., and Jorgensen, R. (1990). Introduction of a chimeric chalcone synthase gene into Petunia results in reversible co-suppression of homologous genes in trans. Plant Cell **2:** 279–289.

Naumann, A., Navarro-González, M., Peddireddi, S., Kües, U., and Polle, A. (2005). Fourier transform infrared microscopy and imaging: Detection of fungi in wood. Fungal Genet. Biol. **42:** 829–835.

Nilsson, O., Moritz, T., Sundberg, B., Sandberg, G., and Olsson, O. (1996). Expression of the *Agrobacterium rhizogenes rol*C gene in a deciduous forest tree alters growth and development and leads to stem fasciation. Plant Physiol. **112:** 493–502.

O'Connell, A., Holt, K., Piquemal, J., Grima-Pettenati, J., Boudet, A., Pollet, B., Lapierre, C., Petit-Conil, M., Schuch, W., and Halpin, C. (2002). Improved paper pulp from plants with suppressed cinnamoyl-CoA reductase or cinnamyl alcohol dehydrogenase. Transgenic Res. **11:** 495–503.

Osakabe, K., Tsao, C.C., Li, L., Popko, J.L., Umezawa, T., Carraway, D.T., Smeltzer, R.H., Joshi, C.P., and Chiang, V.L. (1999). Coniferyl aldehyde 5-hydroxylation and methylation direct syringyl lignin biosynthesis in angiosperms. Proc. Natl. Acad. Sci. USA **96:** 8955–8960.

Oxley, D., and Bacic, A. (1999). Structure of the glycosylphosphatidylinositol anchor of an arabinogalactan protein from *Pyrus communis* suspension-cultured cells. Proc. Natl. Acad. Sci. USA **96:** 14246–14251.

Parameswaran, N., and Liese, W. (1980). Ultrastructural aspects of bamboo cells. Cell. Chem. Technol. **14:** 587–609.

Parameswaran, N., and Liese, W. (1981). Occurrence and structure of polylamellate walls in some lignified cells. In Cell Walls '81, Proceedings of the 2nd Cell Wall Meeting, Göttingen, Germany, April 8–11, 1981, D.G. Robinson and H. Quadar, eds (Stuttgart, Germany: Wissenschaftliche Verlagsgesellschaft), pp. 171–187.

Parameswaran, N., and Liese, W. (1985). Fibre wall architecture in the stem of rotan manau (*Calamus manan*). In Proceedings of the Rattan Seminar, Kuala Lumpur, Malaysia, October 2–4, 1984, K.M. Wong and N. Manokaran, eds (Kepon, Malaysia: Forest Research Institute Malaysia), pp. 123–129.

Peter, G.F., White, D.E., De La Torre, R., Singh, R., and Newman, D. (2007). The value of forest biotechnology: A cost modelling study with loblolly pine and kraft linerboard in the southeastern USA. Int. J. Biotechnol. **9:** 415–435.

Pilate, G., et al. (2002). Field and pulping performances of transgenic trees with altered lignification. Nat. Biotechnol. **20:** 607–612.

Pinçon, G., Chabannes, M., Lapierre, C., Pollet, B., Ruel, K., Joseleau, J.-P., Boudet, A.M., and Legrand, M. (2001). Simultaneous down-regulation of caffeic/5-hydroxy ferulic acid-*O*-methyltransferase I and cinnamoyl-coenzyme A reductase in the progeny

from a cross between tobacco lines homozygous for each transgene. Consequences for plant development and lignin synthesis. Plant Physiol. **126:** 145–155.

Piquemal, J., Lapierre, C., Myton, K., O'Connell, A., Schuch, W., Grima-Pettenati, J., and Boudet, A.-M. (1998). Down-regulation in cinnamoyl-CoA reductase induces significant changes of lignin profiles in transgenic tobacco plants. Plant J. **13:** 71–83.

Raes, J., Rohde, A., Christensen, J.H., Van de Peer, Y., and Boerjan, W. (2003). Genome-wide characterization of the lignification toolbox in Arabidopsis. Plant Physiol. **133:** 1051–1071.

Ralph, J., Akiyama, T., Kim, H., Lu, F., Schatz, P.F., Marita, J.M., Ralph, S.A., Reddy, M.S.S., Chen, F., and Dixon, R.A. (2006). Effects of coumarate-3-hydroxylase down-regulation on lignin structure. J. Biol. Chem. **281:** 8843–8853.

Ralph, J., Brunow, G., and Boerjan, W. (2007a). Lignins. In Encyclopedia of Life Sciences. (Chichester, UK: John Wiley & Sons), http://www.els.net/, doi/10.1002/9780470015902.a0020104.

Ralph, J., Kim, H., Lu, F., Grabber, J., Leplé, J.-C., Sierra, B., Derikvand, M.M., Jouanin, L., Boerjan, W., and Lapierre, C. (2007b). Identification of the structure and origin of a thioacidolysis marker compound for ferulic acid incorporation into angiosperm lignins (and an indicator for cinnamoyl-coA reductase deficiency). Plant J., in press.

Ralph, J., Lundquist, K., Brunow, G., Lu, F., Kim, H., Schatz, P.F., Marita, J.M., Hatfield, R.D., Ralph, S.A., Christensen, J.H., and Boerjan, W. (2004). Lignins: Natural polymers from oxidative coupling of 4-hydroxyphenylpropanoids. Phytochem. Rev. **3:** 29–60.

Ralph, J., et al. (1999). Solution-state NMR of lignins. In Advances in Lignocellulosic Characterization, D.S. Argyropoulos, ed (Atlanta, GA: TAPPI Press), pp. 55–108.

Ranjan, P., Kao, Y.-Y., Jiang, H., Joshi, C.P., Harding, S.A., and Tsai, C.-J. (2004). Suppression subtractive hybridization-mediated transcriptome analysis from multiple tissues of aspen (*Populus tremuloides*) altered in phenylpropanoid metabolism. Planta **219:** 694–704.

Robinson, A.R., Gheneim, R., Kozak, R.A., Ellis, D.D., and Mansfield, S.D. (2005). The potential of metabolite profiling as a selection tool for genotype discrimination in *Populus.* J. Exp. Bot. **56:** 2807–2819.

Roessner, U., Wagner, C., Kopka, J., Trethewey, R.N., and Willmitzer, L. (2000). Simultaneous analysis of metabolites in potato tuber by gas chromatography-mass spectrometry. Plant J. **23:** 131–142.

Rohde, A., et al. (2004). Molecular phenotyping of the *pal1* and *pal2* mutants of *Arabidopsis thaliana* reveals far-reaching consequences on phenylpropanoid, amino acid, and carbohydrate metabolism. Plant Cell **16:** 2749–2771.

Sambrook, J., Fritsch, E.F., and Maniatis, T. (1989). Molecular Cloning: A Laboratory Manual, 2nd ed. (Cold Spring Harbor, NY: Cold Spring Harbor Laboratory Press).

Schauer, N., Steinhauser, D., Strelkov, S., Schomburg, D., Allison, G., Moritz, T., Lundgren, K., Roessner-Tunali, U., Forbes, M.G., Willmitzer, L., Fernie, A.R., and Kopka, J. (2005). GC-MS libraries for the rapid identification of metabolites in complex biological samples. FEBS Lett. **579:** 1332–1337.

Schoch, G., Goepfert, S., Morant, M., Hehn, A., Meyer, D., Ullmann, P., and Werck-Reichhart, D. (2001). CYP98A3 from *Arabidopsis thaliana* is a 3′-hydroxylase of phenolic esters, a missing link in the phenylpropanoid pathway. J. Biol. Chem. **276:** 36566–36574.

Seitz, B., Klos, C., Wurm, M., and Tenhaken, R. (2000). Matrix polysaccharide precursors in *Arabidopsis* cell walls are synthesized by alternate pathways with organ-specific expression patterns. Plant J. **21:** 537–546.

Shi, C., Koch, G., Ouzunova, M., Wenzel, G., Zein, I., and Lübberstedt, T. (2006). Comparison of maize brown-midrib isogenic lines by cellular UV-microspectrophotometry and comparative transcript profiling. Plant Mol. Biol. **62:** 697–714.

Showalter, A.M. (2001). Arabinogalactan-proteins: Structure, expression and function. Cell. Mol. Life Sci. **58:** 1399–1417.

Sjödin, A., Bylesjö, M., Skogström, O., Eriksson, D., Nilsson, P., Rydén, P., Jansson, S., and Karlsson, J. (2006). UPSC-BASE - *Populus* transcriptomics online. Plant J. **48:** 806–817.

Sterky, F., et al. (2004). A *Populus* EST resource for plant functional genomics. Proc. Natl. Acad. Sci. USA **101:** 13951–13956.

Sun, W., Zhao, Z.D., Hare, M.C., Kieliszewski, M.J., and Showalter, A.M. (2004). Tomato LeAGP-1 is a plasma membrane-bound glycosylphosphatidylinositol-anchored arabinogalactan-protein. Physiol. Plant. **120:** 319–327.

TAPPI Useful Method UM-250 (1991). Acid-Soluble Lignin in Wood and Pulp. (Atlanta, GA: Tappi Press).

Taylor, G., Street, N.R., Tricker, P.J., Sjödin, A., Graham, L., Skogström, O., Calfapietra, C., Scarascia-Mugnozza, G., and Jansson, S. (2005). The transcriptome of *Populus* in elevated CO_2. New Phytol. **167:** 143–154.

Terashima, N., Okada, M., and Tomimura, Y. (1979). Heterogeneity in formation of lignin. I. Heterogeneous incorporation of *p*-hydroxybenzoic acid into poplar lignins. Mokuzai Gakkaishi **25:** 422–426.

Thumma, B.R., Nolan, M.F., Evans, R., and Moran, G.F. (2005). Polymorphisms in *cinnamoyl CoA reductase* (*CCR*) are associated with variation in microfibril angle in *Eucalyptus* spp. Genetics **171:** 1257–1265.

Tsai, C.-J., Popko, J.L., Mielke, M.R., Hu, W.-J., Podila, G.K., and Chiang, V.L. (1998). Suppression of *O*-methyltransferase gene by homologous sense transgene in quaking aspen causes red-brown wood phenotypes. Plant Physiol. **117:** 101–112.

Tuskan, G.A., et al. (2006). The genome of black cottonwood, *Populus trichocarpa* (Torr. & Gray ex Brayshaw). Science **313:** 1596–1604.

Wilce, M.C.J., and Parker, M.W. (1994). Structure and function of glutathione *S*-transferases. Biochim. Biophys. Acta **1205:** 1–18.

Wong, H.L., Sakamoto, T., Kawasaki, T., Umemura, K., and Shimamoto, K. (2004). Down-regulation of metallothionein, a reactive oxygen scavenger, by the small GTPase OsRac1 in rice. Plant Physiol. **135:** 1447–1456.

Zhou, A., and Li, J. (2005). *Arabidopsis* BRS1 is a secreted and active serine carboxypeptidase. J. Biol. Chem. **280:** 35554–35561.